CHALMERS
UNIVERSITY OF TECHNOLOGY

E-Band/W-Band Corrugated Horn Feed for the Onsala Space Observatory 20 m Radio Telescope

Antenna Design and Simulation

Master's thesis in Wireless, Photonics and Space Engineering

TASMIAH SHAIKH

Department of Space, Earth and Environment
CHALMERS UNIVERSITY OF TECHNOLOGY
Gothenburg, Sweden 2019

Somewhere, something incredible is waiting to be known

- Carl Sagan

Master's thesis

E-Band/W-Band Corrugated Horn Feed Design for the Onsala Space Observatory 20 m Radio Telescope

Antenna Design and Simulation

TASMIAH SHAIKH

CHALMERS
UNIVERSITY OF TECHNOLOGY

Department of Space, Earth and Environment
Chalmers University of Technology
Gothenburg, Sweden 2019

E-Band/W-Band Corrugated Horn Feed Design for
the Onsala Space Observatory 20 m Radio Telescope
Antenna Design and Simulation
TASMIAH SHAIKH

E-mail: tasmiah.shaikh14@gmail.com Phone: +46 (0) 765526053

Supervisor:Jonas Flygare, Department of Space, Earth and Environment, Onsala Space Observatory and Jian Yang, Department of Electrical Engineering, Chalmers University of Technology
Examiner: Jian Yang, Department of Electrical Engineering, Chalmers University of Technology

Master's Thesis
Department of Space, Earth and Environment
Chalmers University of Technology
SE-412 96 Gothenburg
Telephone: +46 (0)31 772 1000

Onsala Space Observatory
SE-439 92 Onsala
Telephone: +46 (0)31 772 5500

Cover: A cutting-plane view of a corrugated horn feed.

Typeset in LaTeX
Gothenburg, Sweden 2019

E-Band/W-Band Corrugated Horn Feed
for the Onsala Space Observatory 20 m Radio Telescope
Antenna Design and Simulation
Tasmiah Shaikh
Department of Space, Earth and Environment, Onsala Space Observatory
Chalmers University of Technology

Abstract

Radio astronomy is a science which has helped us learn about the universe beyond the one visible to us through naked eyes. Radio telescopes have advanced exponentially since their discovery. The feed of the radio telescope is an important component and its design includes numerous parameters and boundaries. In this thesis we present the design, development, simulation and analysis of a corrugated feed horn for the 20 m reflector type radio telescope located in Onsala Space Observatory, Onsala, Sweden. Corrugated horn is chosen as the feed as it produces low cross-polarization levels and highly symmetric radiation patterns. The corrugated horn feed is designed for frequencies between 70 GHz and 116 GHz (also called the E-/W-Band or the 3mm/4mm Band) with the aim of achieving good aperture efficiency and sensitivity. Requirements were set over the full bandwidth to achieve: input reflection coefficient better than -10 dB, aperture efficiency greater than 50%, sensitivity better than 5500 Jy, and edge tapering of -12 dB at 6.09° half-subtended angle of the sub-reflector. The small half-subtended angle with an edge taper of -12 dB is a challenging design condition.
The design methodology of the horn consists of two steps, first is the design of a smooth wall horn, and second is the design of the corrugated horn. The smooth wall horn is developed to narrow down the variable parameters involved in the design of the corrugated horn. The most promising smooth wall horn candidate is then corrugated and optimized to meet our given specifications. The final successful design meets all the requirements specified. Over the band, input reflection coefficient is found to be better than -16 dB, aperture efficiency averages at 65% and average sensitivity of 2100 Jy when the telescope is unaffected by atmospheric opacity. If we take into account atmospheric opacity, which is the more realistic scenario, then, average maximum sensitivity over the band is found to be 3350 Jy with a peak of 5500 Jy at 70 GHz. The edge-taper at 90 GHz in the $\phi = 0$ plane is found to be -11.356 dB. It is also concluded that an improved mode-converter design can enhance the feed performance in future work. The thesis proves that though the requirement to produce the extremely narrow beam at such high frequencies is challenging, it is not impossible to design a decent corrugated horn feed.

Keywords: antenna, feed, corrugated horn, wideband, e band, w band, radio astronomy, circular horn, antenna simulation, onsala space observatory.

Acknowledgements

I am very grateful to my examiner, Prof. Jian Yang for giving me the opportunity to be a part of this project. Thank you for having faith in me and helping me every time during my studies here at Chalmers. A big thank you to my supervisor, Jonas Flygare, for sharing all that knowledge and for being so very patient with me. I would be very lost without their constant support. I have learned so much in this period of time and I owe it all to you.

I would like to convey my gratitude to my family, Mom, Dad and my little brother Tafazzul, thank you for believing in me and encouraging me through every step of life. Without you, I wouldn't be here at all. I love you all very much and wish you could be here with me.

To my dear friends; Abhishek, Anali and Shirish, thank you for bearing with me through this time and for always being there when I needed someone to talk to. Adarsh and Abhishek, thank you for being my constant supply of coffee, tea and food while writing this report. A very special thank you to Pallavi, even though you were not here, you never failed to give me a new perspective of things at just the right time.

The past year has been a very challenging and difficult time for me both personally and academically. It has taken a tremendous amount of motivation and support from a lot of people to get me through the year and I would like to thank them all for being my pillars of support.

Tasmiah Shaikh, Gothenburg, Month January 2019

Contents

List of Figures

1 Introduction

Curiosity has led humankind to great developments. From the discovery of fire to the invention of computers, we have managed to demystify the world around us. We have lead earth through different eras, seen mass extinctions as well as evolution. The constant through all these ages have been our skies, still full of mystery, intrigue and enigma.

Astronomy is defined as the study of the sun, moon, stars, planets, comets, gas, galaxies, dust and other non-Earthly bodies and phenomena [1]. It has been practiced for as long as we have gazed up at the night sky, towards the millions of twinkling lights wondering what they were and how they came to be. Early civilizations such as the Mayans (Central and South America), Harappans (Indian Sub-continent) and Greeks used the movement of the sun and stars to keep track of time [2]. Ancient Mariners used the position of stars to navigate their way through seas and oceans. Even today, in this modern world, Global Positioning System satellites use distant astronomical objects such as quasars and distant galaxies to determine accurate positions [3].

How is it though that we are able to observe objects in deep space? Ingenious engineering and technological advancements play a big role in the development of any science. The same goes for astronomy. Observations made with the naked eye led Copernicus to put forward his theory of a heliocentric solar system as opposed to the geocentric model first proposed by Ptolemy. More than fifty years after Copernicus's death, Galileo Galilei observed the skies with his invention of a long thin hollow cylindrical tube with lenses placed at either end. This was the first prototype of the modern day refractor telescope [4], [5]. From there, we have developed modern techniques such as spectroscopy and interferometry along with various telescopic observations of the electromagnetic spectrum, have helped us observe, infer and analyze big and small structures spread across our vast universe.

Depending on which section of the electromagnetic spectrum is being studied, astronomy can be broadly classified into radio astronomy, optical astronomy, infrared astronomy and high-energy astronomy which includes X-ray astronomy, gamma ray astronomy and UV astronomy. In this report we present the design, optimization and system analysis of a corrugated feed horn for a Cassegrain reflector telescope for astronomical observations at E- and W-band.

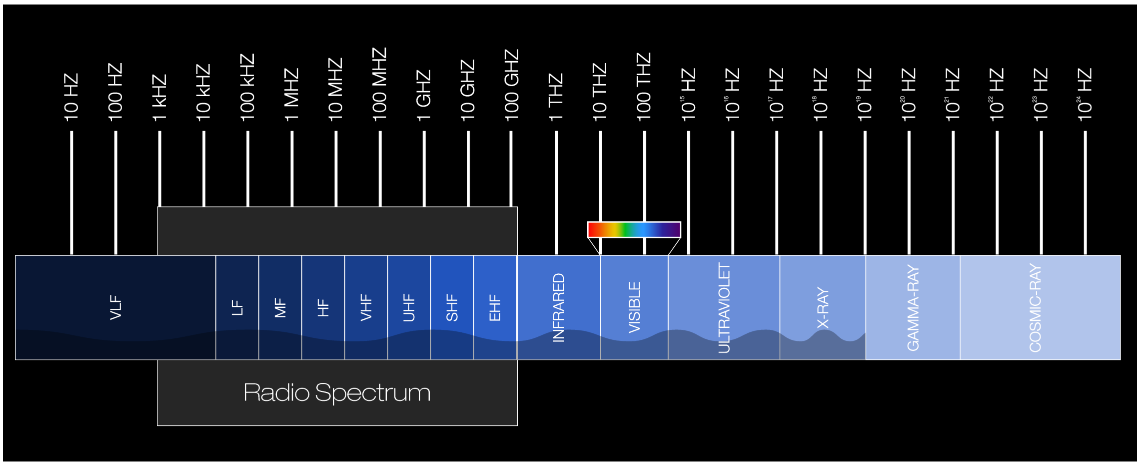

Figure 1.1: The complete electromagnetic spectrum with specification of the area roughly considered as radio waves (Source: NASA [6]).

1.1 Radio Astronomy

Radio astronomy is a branch of astronomy that studies celestial objects that emit radio waves. Radio waves are part of the full electromagnetic spectrum spread across the frequencies from 3 kilohertz up to 300 gigahertz. That is a variation from the size of a tall building to the size of a pinhead in terms of wavelengths. Figure 1.1 shows the complete electromagnetic spectrum ranging from very low frequency up to the cosmic waves region.

Radio Astronomy was born when Karl Jansky in the early 1930's discovered a constant invisible type of noise coming from the skies while doing research work on short radio waves for Bell Laboratories. He built an antenna for 20.5 MHz (14.5 m wavelength) commissioned by Bell Laboratories for his work at the time. He observed that the static signal repeated every 23 hours and 56 minutes and seemed to be coming from a point away from the sun. He found that this static noise was actually coming from the centre of the Milky Way galaxy, specifically from the constellation of Sagittarius. This was the first ever use of radio waves in astronomy. He published his work and got a good deal of attention. From there, the work was picked up by Grote Reber who built the first reflector-type radio telescope in his backyard. It was a 9 m parabolic reflector. Grote set the stage for the boom in radio astronomy after the end of World War II [7], [8]. Since then, radio astronomy and its applications have advanced exponentially from the discovery of the cosmic microwave background radiation (CMBR), hundreds of radio galaxies, the discovery of pulsars and binary pulsars to observation of the spiral structure of our galaxy from HI 21 cm emission. Radio astronomy has helped us learn so much about the universe we can't see with visible light. Today, ultra-sensitive high-frequency millimetre-wave (mm-wave) radio telescopes as well as very low frequency radio telescopes are decoding the mysteries of the beginning of our universe. Figure 1.2 shows an excellent example of an astronomical structure imaged at three different frequencies.

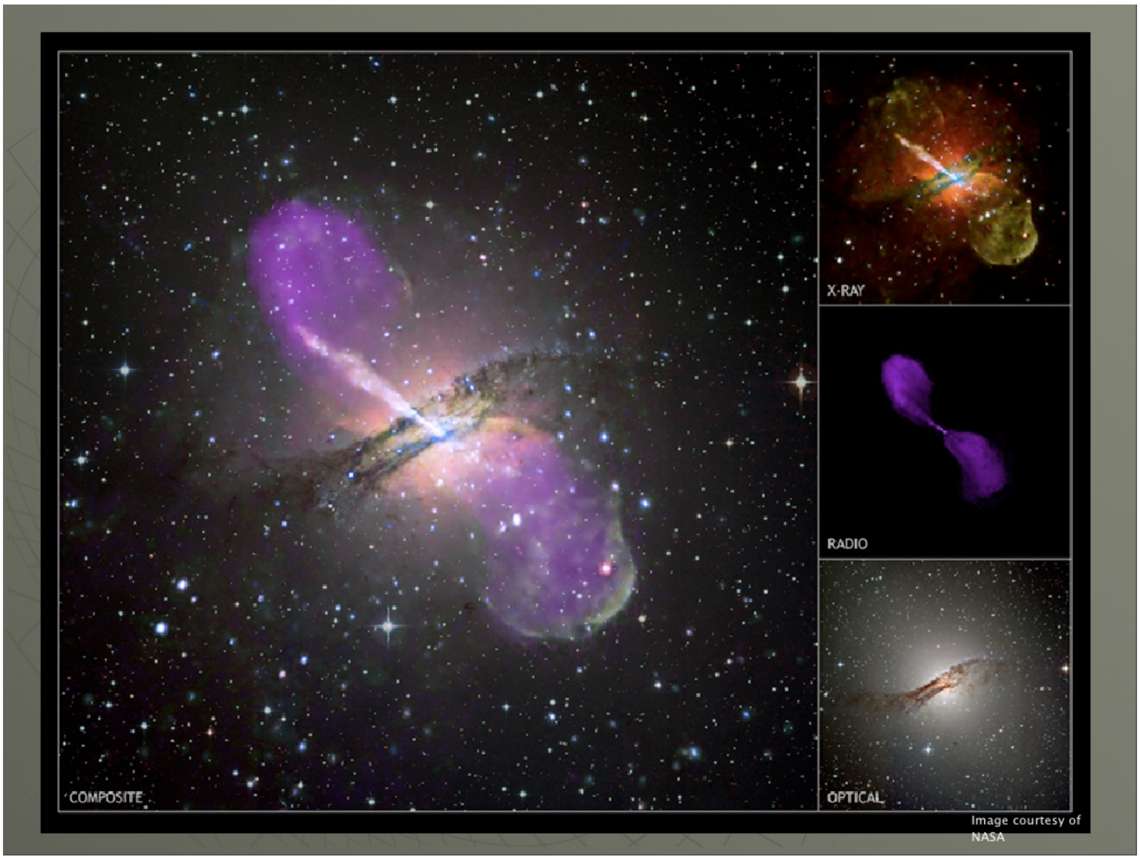

Figure 1.2: This image shows Centaurus A, a radio active galaxy. The main image shows a composite made of three different images taken at different wavelengths. The top-right image is taken from the Chandra X-ray observatory and shows high-energy emissions from a super-massive black hole hidden in the bands of dust in the center. The radio image shows humongous jets pushed into space, these are radio lobes and the optical image shows thick dust clouds obstructing light coming from the millions of stars in the galaxy (Source: NASA [9]).

1.1.1 E-W Band in Radio Astronomy

Frequencies in the range between 60 GHz to 116 GHz (E- and W-band) are very important in radio astronomy. This frequency range is often called the 3mm/4mm band due to it's approximate wavelengths of observation. Radio emissions from the Sun and the moon are studied at 4 mm. The band also spans several important spectral lines that are used to determine the composition of celestial objects. For example, the SiO (Silicon monoxide) maser emission line at 86.2 GHz is used to measure and calibrate telescope performance. CO at 115.271 GHz and ^{13}CO at 110.201 GHz have strong and easily detectable line intensities. These molecules are important as they have a long lifetime as well as consist of two elements found in abundance in the universe - carbon and oxygen. They act as a marker to show regions in outer systems where HI is getting converted to molecular hydrogen. Apart from these molecules, there are many other elements that can be detected in this band, the full list is available at [10].

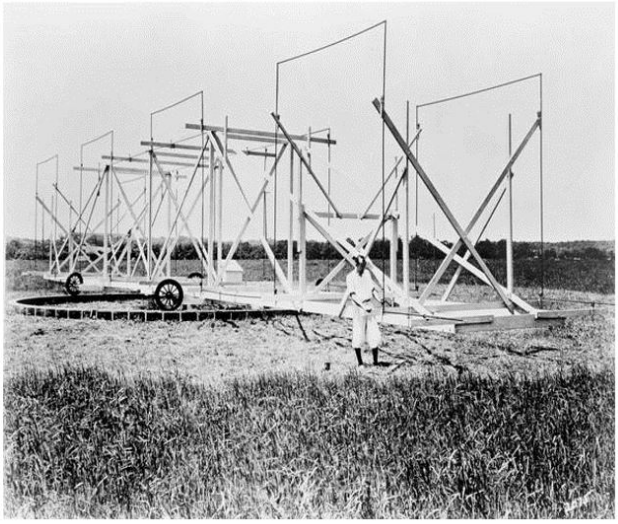

(a)

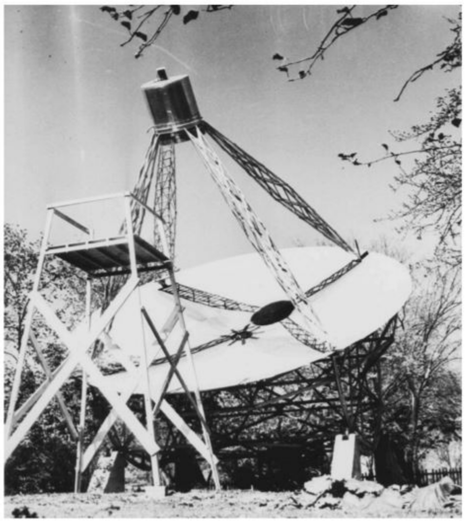

(b)

Figure 1.3: Early radio telescopes:(a) shows the 20 MHz antenna that Karl Jansky used to make his discovery about radio emissions coming from the Milky Way galaxy (Source: NRAO [7]); (b) shows the first radio telescope, a 9 m parabolic reflector, built by Reber Grote (Source: Astronomy Today [8]).

1.2 Onsala Space Observatory

Onsala Space Observatory (OSO) [11] is the Swedish National facility for Radio Astronomy. Located roughly 45 km south of the city of Göteborg in Sweden, it operates several telescopes for astronomy and geodesy. The observatory was founded by Prof. Olof Rydbeck in 1949 and is hosted and run on behalf of the Swedish Research Council by the Department of Space, Earth and Environment at Chalmers University of Technology.

The infrastructure within the observatory consists of many different instruments for observational sciences. The 20 and 25 m telescopes are mostly used for astronomical purposes. They study the birth and death of stars and look at molecules from the Milky Way and other galaxies. LOFAR or the Low Frequency Array is part of an international network of antennas that study the origins of our universe as well as pulsars. The Onsala Twin Telescopes (OTT) are the latest addition to the observatory. These 13.2 m twin radio telescopes are dedicated to the next generation of geodetic very long baseline interferometry (VLBI) observations. They are part of the VLBI global observing system (VGOS) with the goal of improving the global positioning systems' precision to millimeter level. SALSA (Such a Lovely Small Antenna) are 2.3 m radio telescopes which are used to introduce radio astronomy to students and teachers alike. The observatory also has gravimeters, tide gauges and radiometers which are used to study movements in the Earth's crust, sea level, and the rotation of the earth. It also houses two hydrogen maser clocks as well as a cesium clock that establishes the official Swedish time and international time. The 25 m radio telescope was the first of its kind in Europe and is part of a worldwide network of antennas used for VLBI observations. Onsala Space Observatory has developed instruments and is part of the observation crew for the Atacama Pathfinder Experiment (APEX) and Atacama Large Millimeter/sub-millimeter Array (ALMA) located on the Atacama desert plateau in Chile. Onsala has also contributed to the technical development of instruments for the Square Kilometre Array (SKA), which will be the largest and most sensitive telescope in the world for meter and centimeter wavelengths. Figure 1.4 show some of the above mentioned radio telescopes.

1.3 Scope of the Thesis

This project was a collaboration between the antenna systems group at E2 and Onsala at SEE. This thesis presents the design, development and simulation of an E-W band corrugated feed horn for the 20 m reflector telescope at Onsala. This thesis is a step towards the development of a multi-pixel feed or 'radio-camera' for the 20 m dish. Due to time constraints, the work was limited to the design of a single feed element and the evaluation of its performance. To design a radio-camera further work is needed, but this will not be discussed in this thesis.

The report starts with Chapter 1 giving a brief introduction about astronomy and radio astronomy in particular, and the Onsala Space Observatory. Chapter 2 describes the basic theory behind antenna design and Chapter 3 describes the specifications and requirements of this project. The design methodology and optimization process has been described in Chapter 4 and the results have been reported and discussed in Chapter 5. The thesis is concluded in Chapter 6 and ends in Chapter 7 with possible future work. Only theory directly relevant for this project has been introduced to limit the size of the thesis.

1.3.1 Software

CST Microwave Studios [12] and Mathworks Inc. MATLAB [13] were the main softwares used for this project. CST Microwave Studio was used for electromagnetic design and simulation of the feed horn whereas MATLAB served as a computational tool that helped in the design and optimization of corrugations in the feed horn as well as system performance calculations.

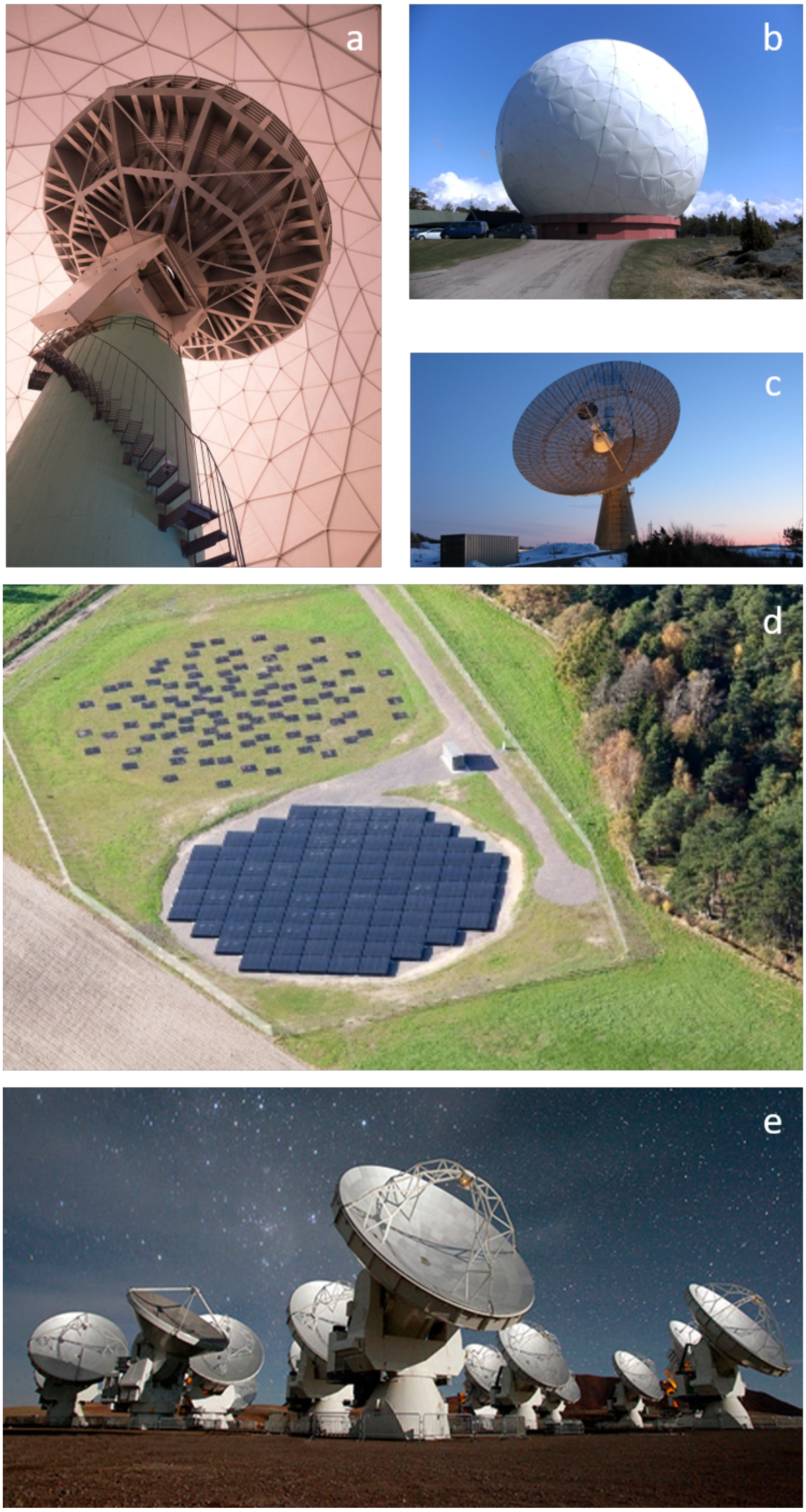

Figure 1.4: Onsala Space Observatory Telescopes:(a) & (b) show the 20 m dish from outside and inside of the radome; (c) 25 m dish; (d) LOFAR cluster; (e) ALMA in the Atacama Desert, Chile (Source: OSO [11]).

2

Theoretical Background

In this chapter we discuss theoretical concepts that form the background of this thesis. We talk about some basic antenna theory, reflector systems, corrugation theory and how all of these play a role in radio astronomy.

Several standard references have been used for antenna theory and design in this thesis [14], [15], [16]. Most of the information provided in this chapter about antenna theory is majorly obtained from these three textbooks. A special reference goes to the master thesis written by Jonas Flygare [17], the report was used as a reference to understand technical concepts in very simple language. We also look at the theory behind corrugations and why corrugated horns are commonly used as feeds for parabolic reflectors. Lastly, we discuss some concepts of astronomy that explain what radio telescopes actually see during observations.

2.1 Basics of Antenna Theory

Antenna theory is a very broad subject matter. For convenience we mention the general properties which are applicable to most antennas and relevant to this project. The equations shown in the matter are not necessarily used in calculations in this project but are shown here for understanding the theory behind basic concepts.

2.1.1 Far-field Approximation

An antenna is defined as a device used for radiating or receiving electromagnetic radiation. Depending on the distance at which the radiation of the antenna is measured, different radiation fields exist, namely, reactive near-field region, radiative near-field region and far-field region. In this project, we only use the far-field region as distances at which sources are observed in radio astronomy are extremely large. The far-field region is defined as,

$$r \geq \frac{2D^2}{\lambda} \tag{2.1}$$

where,
r = distance from the antenna at which radiation field is being measured;
D = largest linear dimension of the antenna;
λ = corresponding wavelength;
A radiating source like the antenna or in our case, a distant star would produce spherical waves spreading in all directions. In the far-field region, however, these

spherical waves can be approximated to be planar. This is a good approximation that simplifies calculations.

2.1.2 Reciprocity

The reciprocity theorem of antennas, states that the properties of a transmitting antenna and those of a receiving antenna are identical. If we know how the antenna is going to perform in one state, we can infer its performance in the other. This is only valid for a linear-type antenna in a linear medium, which fortunately is the case of the antenna design and application of this thesis. In general, antennas are discussed in terms of "transmitting mode" due to the applicability of the nomenclature, even if the application is for a receiving antenna which is the case in radio astronomy.

2.1.3 Bandwidth

The bandwidth of an antenna is defined as the difference between its highest and lowest operating frequency.

$$B = f_{max} - f_{min} \tag{2.2}$$

where, f_{max} = maximum operating frequency and f_{min} = lowest operating frequency. For wideband antennas, like in our case, bandwidth is defined as a ratio,

$$B = \frac{f_{max}}{f_{min}} \tag{2.3}$$

The bandwidth is then expressed as B:1 bandwidth.

2.1.4 Polarization and Antenna Coordinate System

Polarization of an antenna is defined as the polarization of the wave radiated by the antenna. Antenna polarization can be expressed in two components: co-polarization and cross-polarization. Co-polarization is the desired polarization component and cross-polarization is the undesired component of far-field radiation. Tha antenna often has specifications that require minimization of the antenna cross-polarization. Polarization can be linear, circular or elliptical. In this thesis the antenna application desires dual-linear polarization.

Antenna measurements often use the spherical coordinate system as a reference for measurements. Ludwig's 3^{rd} definition can be used in this system to describe polarization in terms of base vectors $\hat{x}$ and $\hat{y}$

$$\begin{aligned} \hat{x} &= cos\varphi\,\hat{\theta} - sin\varphi\,\hat{\varphi} \\ \hat{y} &= sin\varphi\,\hat{\theta} + cos\varphi\,\hat{\varphi} \end{aligned} \tag{2.4}$$

2.1.5 Radiation Pattern

The radiation pattern of an antenna is defined by its E-Field and can be represented in an equation as,

$$E(r, \theta, \phi) = \frac{e^{-jkr}}{r} G(\theta, \phi) \tag{2.5}$$

where, r is the distance from the antenna, e^{-jkr} is the phase component of the antenna and $G(\theta, \phi)$ is the far-field function that gives the direction and phase of the field. When an antenna is used as a feed in a parabolic reflector, (2.5) can be written as

$$E_{feed}(p, \theta, \phi) = \frac{e^{-jkp}}{r} G_{feed}(\theta, \phi) \tag{2.6}$$

where, p is the distance from the feed to the reflector surface [18].

2.1.6 Antenna Gain and Directivity

Antenna Gain, G, also called realized gain or power gain or simply gain is defined as the ratio of intensity radiating in a given direction to the intensity of an isotropically radiating antenna [15]. It can be written as,

$$G = 4\pi \frac{radiation\ intensity}{total\ accepted\ power} = 4\pi \frac{U(\theta, \phi)}{P_{in}}. \tag{2.7}$$

The directivity, D, of an antenna is defined as the ratio of intensity radiating in a given direction to the radiation intensity averaged over all directions [15].

$$D = 4\pi \frac{radiation\ intensity}{average\ radiated\ power} = 4\pi \frac{U(\theta, \phi)}{P_{rad}}. \tag{2.8}$$

Though the definitions for both gain and directivity seem very similar, they are not the same entity. According to IEEE standards, gain accounts for conduction and dielectric losses in the antenna. According to the definition given in [15], gain includes the dielectric and conduction losses as well as losses due to mismatch between the transmission line and the antenna, dielectric. In this thesis, all the results presented are measured in gain defined according to the IEEE standard. The directivity of the antenna is calculated from the radiation pattern of the antenna and does not take into account the various losses of the antenna. The quantities are related through the following equation,

$$G = \eta_{rad} \eta_{pol} D \tag{2.9}$$

where, η_{rad} is the total radiation efficiency of the antenna and η_{pol} is the polarization efficiency of the antenna. These efficiencies along with others, have been elaborated on in the next Section 2.1.7.

2.1.7 Effective Area, Antenna Efficiency and Aperture Illumination Efficiency

The effective aperture area, A_{eff}, of an antenna is defined as the ratio between the total power, P_r, received at the antenna port and power density, W_t, of the plane wave coming in from the direction towards which the antenna has been pointed [14].

$$A_{eff} = \frac{P_r}{W_t} \tag{2.10}$$

Effective area can also be equated in relation to the gain, G, of the antenna as,

$$A_{eff} = \frac{\lambda^2}{4\pi} G \tag{2.11}$$

A number of efficiencies are associated to the design of the antenna. These take into account losses in the antenna that occur due to mismatch between the transmission line and the antenna (η_{mis} = 1 - $|\Gamma|^2$), where Γ is the reflection coefficient), and radiation losses such as conduction loss (η_c) and dielectric losses (η_d). Efficiencies η_c and η_d make-up the antenna radiation efficiency, η_{abs}, which along with η_{mis} make up the total radiation efficiency, η_{rad}, to give,

$$\eta_{rad} = \eta_{mis}\eta_c\eta_d = \eta_{mis}\eta_{abs}. \tag{2.12}$$

Aperture illumination efficiency, η_a, is defined as the ratio between the directivity, D, of a planar aperture to the standard directivity, D_{ref}, which is calculated when the same planar aperture is excited with a uniform amplitude and equi-phased distribution,

$$\eta_a = \frac{D}{D_{std}}. \tag{2.13}$$

When the planar aperture's geometrical area, A_{geom} » λ^2, then,

$$D_{std} = \frac{4\pi}{\lambda^2} A_{geom}, \tag{2.14}$$

which, with (2.13), gives us,

$$\eta_a = \frac{\lambda^2}{4\pi} \frac{D}{A_{geom}}. \tag{2.15}$$

Polarization loss due to mismatch in the polarization of the of the antenna and the polarization of the incoming radiation is accounted for as polarization efficiency, η_{pol}. This efficiency is not always included in the calculation of total antenna efficiency. The total antenna efficiency is then given as,

$$\eta_{ant} = \eta_{rad}\eta_a\eta_{pol}. \tag{2.16}$$

Rearranging (2.9), (2.11) and (2.15), we observe a relation between the total antenna efficiency and effective and geometric areas of the antenna as,

$$\eta_{ant} = \frac{A_{eff}}{A_{geom}}. \tag{2.17}$$

2.2 Brightness Temperature

If our eyes could see the sky at radio wavelengths, the following image represents what the sky would look like,

Figure 2.1: The sky at radio wavelengths if they were visible to our naked eyes (Source: NRAO/ NSF [19]).

Brightness temperature, T_b, of a source is defined as the equivalent temperature that a black body would have to achieve at a given frequency, in order to be as bright as it appears in intensity. Planck's Law of black-body radiation is given as,

$$I(f,T) = \frac{2hf^3}{c^2}\frac{1}{e^{\frac{hf}{k_BT}}-1} \qquad \left(\frac{Jy}{sr}.10^{26}\right) \tag{2.18}$$

where, $I(f,T)$ is the spectral radiance of the body at frequency f and thermal equilibrium temperature T, h is Planck's constant, c is the speed of light and k_B is the Boltzmann's constant. A perfect black body is an object that absorbs all incident electromagnetic radiation and is opaque or optically thick (the opposite being transparent or optically thin), and non-reflective. In the case where the black body is not perfect and is optically thin, its emission will appear weaker due to lowered intensity. The optical thickness of a source depends on the frequency. In radio astronomy, most sources are optically thick at low frequencies whereas at high frequencies, they are optically thin. Brightness temperature is then estimated by applying the Rayleigh-Jeans limit at low frequencies or high temperatures, $fh \ll k_BT$, to Planck's law. This gives us,

$$I(f,T_b) \approx \frac{2k_B f^2 T_b}{c^2} \qquad \left(\frac{Jy}{sr}.10^{26}\right) \tag{2.19}$$

$$T_b(I,f) = \frac{Ic^2}{2k_B f^2} = \frac{l\lambda^2}{2k_B} \qquad (K) \tag{2.20}$$

This brightness temperature is what radio telescopes 'see' through their apertures. Each observation is done continuously for a set period of time in order to collect enough light intensity for decipherable data [20]. The brightness temperature is not an actual physical temperature though, it can be related to the physical temperature as

$$T_b(I,f) = T_{phy}\epsilon \tag{2.21}$$

where, T_{phy} is the physical temperature, and ϵ is the emissivity of the source being observed.

2.3 System Noise Temperature

Radio telescopes measure faint signals coming from sources which are millions of kilometres away. It is essential for the detection of this faint signal that all other forms of noise be kept to a minimum. We refer to this noise power in terms of equivalent noise temperature, T, and can be measured as,

$$P_n = k_B T \Delta f \tag{2.22}$$

where, k_B is Boltzmann's constant and Δf is the bandwidth of the system. There are a lot of noise contributors for an antenna system, like noise from microwave and galactic backgrounds, noise from atmospheric emissions, noise due to scattering or spillover of radiation to the ground, noise due to losses in the feed and due to the receiver itself. These can be grouped together as noise from the antenna and noise from the receiver. The system noise temperature, T_{sys} is the estimated as

$$T_{sys} = T_{ant} + T_{rec} \tag{2.23}$$

For a telescope pointing in a specific direction in the sky, the noise in terms of temperature distribution can be defined as,

$$T(\theta,\phi,f) = \begin{cases} T_b(\theta,\phi,f) & 0^\circ \leq |\theta| < 90^\circ \\ T_g(\theta,\phi,f) & 90^\circ \leq |\theta| < 180^\circ \end{cases} \tag{2.24}$$

where, θ is the elevation angle, ϕ is the azimuth angle and f is the frequency. T_b is the surrounding brightness temperature. T_g is considered the ground temperature and is calculated as

$$T_g(\theta,\phi,f) = (1-|\Gamma_g|^2)T_{phy} + |\Gamma_g|^2 T_s(\theta,\phi,f) \tag{2.25}$$

where, Γ_g is the reflection coefficient of the ground and T_{phy} is the physical temperature of the ground. For the purpose of this thesis, we approximate T_g=T_{phy}=290 K. The surrounding brightness temperature has contributions from molecules in the atmosphere as well as microwave and galactic emissions. Generally, noise from the ground is the largest contributor of spill-over, however this is very frequency dependent. At low frequencies, the ground temperature is generally higher and consideration is spill-over is very important. At higher frequencies, like at 70 GHz, the noise temperature from the sky is higher and hence, contributions from ground spill-over becomes less important. Hence, we define, antenna noise temperature, T_A, at $\theta = \theta_p$, where θ_p is the zenith angle, can then be calculated as,

$$T_A = \frac{\iint_{4\pi} G(\theta_p, \phi, f)T(\theta_p, \phi, f)sin\theta_p d\theta_p d\phi}{\iint_{4\pi} G(\theta_p, \phi, f)sin\theta_p d\theta_p d\phi} \tag{2.26}$$

which can then be approximated as,

$$T_A = T_s\eta_{sp} + T_g(1 - \eta_{sp}) \tag{2.27}$$

where, η_{sp} is the spill-over efficiency. This value of T_A is generally obtained by doing a full-sphere integral simulation, however in this thesis we approximate this value of antenna noise temperature. Taking all the equations and losses mentioned in this section into account, the total system noise temperature can be written as,

$$T_{sys} = \eta_{rad}T_A + (1 - \eta_{rad})T_{phy} + T_{REC} \tag{2.28}$$

2.4 Sensitivity and SEFD

Sensitivity of a radio telescope is it's ability to detect radio emissions coming from weak sources. It depends on the effective area and total system noise temperature of a telescope as well as the time duration of observation. It also depends on receiver bandwidth for broadband continuum observations [21].
In this thesis, we use System Equivalent Flux Density (SEFD) as a measure of the sensitivity of the system. It can be mathematically represented as,

$$SEFD = \frac{T_{sys}}{A_{eff}/2k_B} = \frac{2k_B T_{sys}}{A_{eff}} \qquad (Jy) \tag{2.29}$$

where, T_{sys} is the total system noise temperature, A_{eff} is the effective area of the aperture and k_B is Boltzmann's constant. SEFD is measured in the units of Jansky, which is also the unit used to measure the spectral flux density of a distant source. For an unresolved source with a known spectral flux density, S_ν, this greatly simplifies the calculation of integration time for a given signal-to-noise ratio (SNR).

$$\frac{S}{N} = \frac{S_\nu}{SEFD}\sqrt{\tau\Delta\nu} \tag{2.30}$$

The lower the SEFD value is, better the sensitivity of the system [22].

2.5 Reflector Antennas

One of the most common type of antenna used for radio astronomical observations is the reflector antenna. There are many different kinds of reflector antennas with the most popular one being the parabolic reflector antenna. Reflector antennas generally consist of a primary reflector and one or more sub-reflectors. The main concept of these reflectors is to collect the maximum amount of incident radiation and concentrate it towards the feed antenna which may or may not be located on the focal axis of the primary reflector. The feed antenna can be a single element or it can be an array of antennas called the feed array, depending on the application the reflector antenna is used for. Reflector antennas are classified into different types based on the configuration of its main reflector, sub-reflector and feed system. In this thesis, we only focus on the Cassegrain type configuration which is the style of the 20 m dish in Onsala.

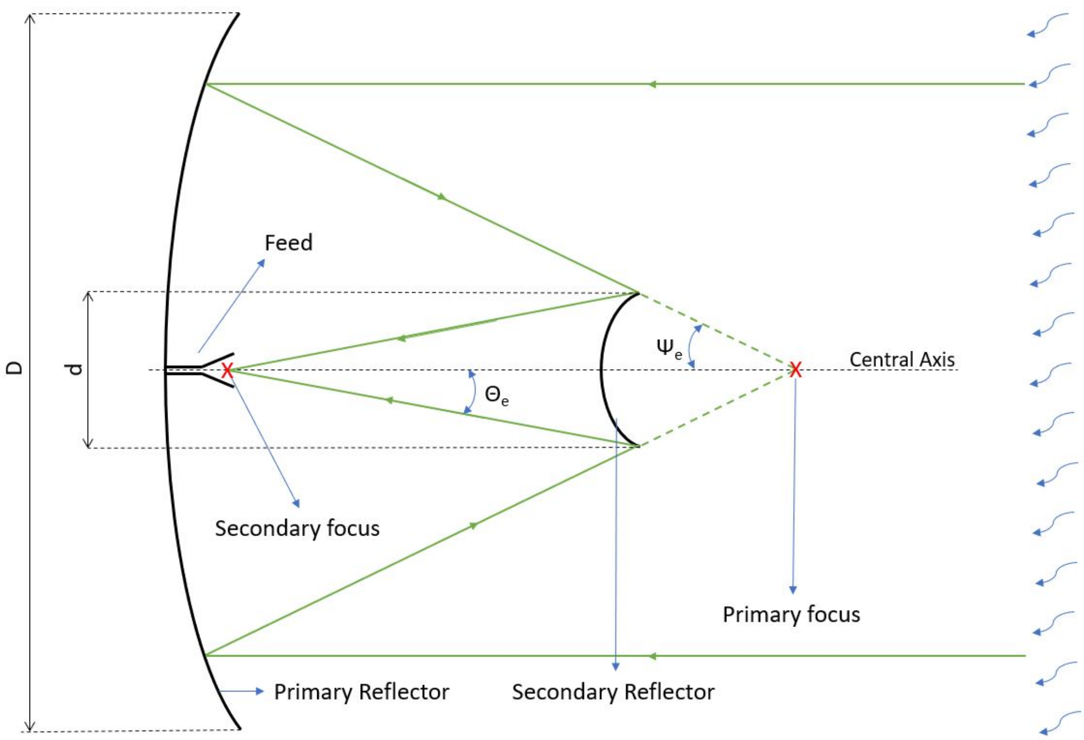

Figure 2.2: Illustration of the geometry of a Cassegrain-type reflector antenna showing main parameters that describe the geometry.

2.5.1 Cassegrain Antenna

The Cassegrain configuration reflector antenna consists of a paraboloidal primary reflector and a hyperboloidal or concave curved sub-reflector. Figure 2.2 is an illustration of the basic geometry of the Cassegrain antenna. D, is the linear diameter of the primary reflector, d is the linear diameter of the secondary reflector, ψ_e is the half-subtended angle of the primary and θ_e is the half-subtended angle of the sub-reflector. Half subtended angle of the sub-reflector, θ_e, is the most important parameter in this thesis as a constraint for the feed design. Due to the sub-reflector-feed system being directly over the primary reflector and in the way of incoming radiation, Cassegrain antennas have some blockage loss that deteriorates the blockage efficiency (η_{block}) of the reflector. The blocked radiation is scattered and contributes to the spill-over loss (η_{sp}). This blockage also hinders the illumination of the reflector and negatively affects the taper illumination efficiency (η_{ill}) of the antenna. For good electrical performance, all these losses must be kept to a minimum, one way is to design the feed pattern to comply with the edge-taper of the reflectors.

2.5.2 Parabolic Dish Efficiencies

The aperture efficiency calculation of a complete reflector-feed antenna system should include the various efficiencies and sub-efficiencies related to the feed and the dish alike. Some of the efficiencies which depend on the feed are discussed in Section 2.1.7. The feed aperture efficiency is defined as,

$$\eta_a = \eta_{sp}\eta_{ill}\eta_{pol}\eta_{ph}\eta_{BOR_1}. \tag{2.31}$$

The first efficiency is the spill-over efficiency, η_{sp}, which gives a measure of the amount of radiated power hitting the surface of the reflector from the total amount of radiated power. η_{pol} is the polarization side-lobe efficiency which gives the amount of power lost in cross-polar sidelobes within the half-subtended angle of the sub-reflector. Aperture illumination efficiency, η_{ill}, gives a measure of how well the power is illuminated over the dish relative to uniform illumination distribution. Phase efficiency, η_{ph} shows the mismatch between the focus of the dish and the phase centre of the feed. η_{BOR_1} is the Body-of-Revolution-1 (BOR_1) sub-efficiency. To obtain maximum secondary gain, only first order azimuthal terms are used in the feed radiation pattern definition (2.6), as higher order azimuthal terms do not contribute to the on-axis gain of the antenna and are hence, presented as a loss. The ratio of power in the first-order azimuthal modes to total radiated power is quantified in the BOR_1 efficiency, also called the azimuth mode efficiency [23], [24]. The mutual dependence of the illumination efficiency, η_{ill} and the spillover efficiency, η_{sp}, give rise to an interesting observation. If the reflector is illuminated with a high edge-taper, η_{ill} becomes close to 100%. However, this greatly increases the power lost to spill-over noise. Hence, a trade-off is required between these two quantities in order to achieve a satisfactory value of aperture efficiency. Figure 3.5 shows an example of the trade-off between both these efficiencies. This example is taken from [14], which is an excellent source to learn about antenna design and engineering.

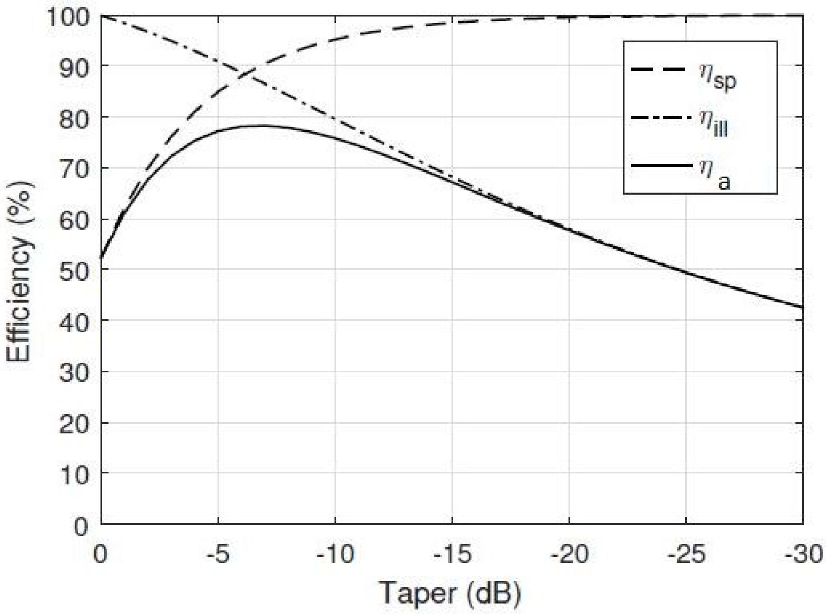

Figure 2.3: An example from [14] that illustrates the trade-off between illumination and spillover efficiency as a product in aperture efficiency calculations.

The sub-efficiencies of the dish can be listed as follows,

$$\eta_{dish} = \eta_{block}\eta_{jitt}\eta_{trans}\eta_{surf}\eta_{disdish} \tag{2.32}$$

where,
η_{block} = blockage efficiency,
η_{jitt} = pointing efficiency due to jitter,
η_{trans} = dish transparency efficiency,
η_{surf} = dish surface efficiency,
$\eta_{disdish}$ = dish dissipation efficiency.

The dish blockage efficiency, η_{block}, gives a measure of how much of the aperture of the dish is blocked due to the sub-reflector and feed structures. Atmospheric aberrations on a day-to-day basis interfere with the pointing direction of the dish, this contributes towards the pointing efficiency of the dish. The continuity of the dish surface (how smooth or rough the surface of the dish is) affects the dish surface efficiency, η_{surf} and the transparency of the aperture is measured by the dish transparency efficiency, η_{trans}. The reflector dish's dissipative losses are quantified using the dish dissipation efficiency, $\eta_{disdish}$. The antenna efficiency of the total telescope system can be now written as a combination of (2.31) and (2.32),

$$\eta_{ant} = \eta_{block}\eta_{jitt}\eta_{trans}\eta_{surf}\eta_{disdish}\eta_{sp}\eta_{ill}\eta_{pol}\eta_{ph}\eta_{dis}\eta_{BOR1}. \tag{2.33}$$

Practically, it is complicated to compute all these efficiencies for the scope of this thesis. Therefore, we calculate the aperture efficiency of the entire system using physical optics (PO) and equations (2.15) and (2.17) from Section 2.1.7.

2.6 Horn Antennas

Horn antennas are most commonly used as feeds in radio-astronomical instruments. The purely metal structure makes them straightforward and not so expensive to manufacture, as well as having low losses. Horn antennas have low side-lobe levels and can perform over a wide bandwidth. Various types of horns exist like conical horns, rectangular horns, sectoral horns and corrugated horns. In the following sections we cover basic corrugation theory and motivate our choice to design a corrugated horn for this thesis.

2.6.1 Corrugated Horn Antennas and Theory

Corrugated horn antennas are the most commonly used as feeds in parabolic reflectors. They were first developed by A.F. Kay in the 1960's and have been improved into high-performing antennas. They have very low cross-polarization levels relative to other horn types and highly symmetrical beam patterns. These characteristics are desired for dual-polarization operation. We will here explain in an intuitive way why corrugations improve the feed performance [25].

The introduction of corrugation in a horn antenna changes its field pattern. To attain axial beam-symmetry and low cross-polarization, the aperture electric field of the horn should be almost linear. 'Almost linear' is used due to the fact that to cancel all components of cross-polarisation, a slight curvature is needed in the walls of the horn. This required linear electric field cannot be produced by horn which only support the standard transverse-electric (TE) or transverse-magnetic modes (TM), which have curved aperture fields. However, a combination of TE and TM modes, also known as hybrid mode, is observed to produce the required linear aperture field. The electric fields produced in a hybrid-mode waveguide is given by,

$$\begin{aligned} E_x &= A_1 J_0(Kr) - \frac{(X-Y)}{kr_1} A_2 J_2(Kr) cos2\phi \\ E_y &= \frac{(X-Y)}{kr_1} A_2 J_2(Kr) sin2\phi \end{aligned} \tag{2.34}$$

where, $J_0(kr)$ and $J_2(kr)$ are Bessel functions of the first kind, K and k are the transverse and free-space wavenumbers, amplitude coefficients are given by A_1 and A_2. X and Y are the impedance and admittance at the boundary of the horn wall defined by r=r_1. For the hybrid mode to propagate within the horn, these impedance and admittance values must be finite and equal or must be zero. The corrugations in the wall of the horn produces these required conditions and the horn is said to be in a 'balanced hybrid mode' which produces the desired characteristics of pattern symmetry and low cross polarization levels. More about the design of the corrugated horn is discussed in Chapter 4.

3

Specifications and Requirements

Every scientific project is defined by some boundaries or constraints. In this chapter, we mention the design goals that need to be met for this thesis project. The evaluation and theory of these goals for this thesis work are evaluated in Chapter 4 and Chapter 2 respectively.

3.1 20 m Dish

The intended reflector dish for the feed design presented in this thesis is the Onsala 20 m telescope. The largest linear diameter, D, of the dish stands at 20.1 m. It has a Schmidt-Cassegrain type sub-reflector mount and is protected by a radome. The half-subtended angle of the sub-reflector is 6.09°. Henceforth, we refer to this reflector dish as the 20 m dish. For more specifications, see [26].

3.2 Bandwidth

The frequency band used for this project is 70–116 GHz also referred to as the 3mm/4mm band. According to section 2.1.3, the specified bandwidth of the feed is,

$$B = \frac{116}{70} = 1.66 : 1 \tag{3.1}$$

3.3 S-parameters

For radio astronomy receiver integration of a wideband feed, the feed reflection coefficient should be less than -10 dB as a minimum. Therefore, the optimization requirement on the reflection coefficient was strictly set to $\mid S_{11} \mid <$ -10 dB.

3.4 Radiation Efficiency

Radiation efficiency of an antenna tells us how effective an antenna is at converting the accepted power to radiated power (or receiver power to output power at the port). For this type of pure-metal feed structure, the radiation efficiency is expected to be very close to 100% [15].

3.5 Aperture Efficiency

Most radio telescopes have aperture efficiency $\eta_A \leq 70\%$ according to section 3.3.2 of [27]. Aperture efficiency is one of the figures-of-merit of this thesis. The goal for this design is to achieve a minimum of $\eta_A \geq 50\%$ across the frequency band.

3.6 Beam width and Edge Taper

The Onsala 20 m radio telescope has a very narrow half-subtended opening angle of the sub-reflector of $\theta_e = 6.09°$. In order to achieve a high value of aperture efficiency while also maintaining a low spill-over noise contribution, the desired edge taper at θ_e is chosen to be -12 dB. This means that the antenna should have a gain drop of -12 dB at 6.09° in order to satisfy the aperture efficiency requirement.

3.7 Sensitivity and System Equivalent Flux Density (SEFD)

Sensitivity of a radio telescope is often used as it's figure-of-merit. In this thesis, we use SEFD as one of our figures-of-merit and as a measure of sensitivity of the system. It gives us a direct comparison in terms of the strength of the source we observe. We aim to have a low SEFD number so as to achieve high sensitivity. According to pp. 36 of [28] the current EW band receiver has a SEFD number approximately between 5000 and 6000 Jy. Our aim is to achieve a SEFD number lower than 5500 Jy.

4

Design Methodology and Parameters

In this chapter, we talk about the design methodology used to reach the final design of the corrugated feed horn. The design was done in two different stages: smooth wall horn design and corrugated horn design.
Each stage had its own optimization runs. For the smooth wall horn stage the optimization software used was CST Microwave Studio and for the corrugated horn stage, the optimization was performed with MATLAB. The design procedure of the corrugated feed was mostly based on the standard reference paper titled: "Design of Corrugated Horns: A Primer" by Christophe Granet and Graeme L. James [29]. Other papers were also used and will be cited appropriately throughout this chapter.

4.1 Smooth Wall Horn

A conical horn was used as a base design for this project. The horn would be connected to a circular waveguide which would 'feed' the receiver with all the radiation collected from the main parabolic reflector and sub-reflector. For the base design of the key parameters of the horn, we follow the considerations mentioned in the Granet paper [29]. The main parameters of the smooth wall horn consist of the lowest and highest input frequency, the center frequency, output frequency, input radius, output radius, length of the horn and profile of the horn.

4.1.1 Design Frequencies

Four different frequency parameters are used in the horn design, these are:

- f_{min}: the lowest operating frequency
- f_{max}: the highest operating frequency
- f_c : the center frequency,we observe most of our results at this frequency (Wavelength λ_c)
- f_{out} : the output frequency (wavelength λ_0)

In some literature, f_0 denotes the center frequency, however in [29], it is denoted with f_c. For clarity, we also use f_c when denoting the center frequency. For narrowband applications, the ratio between f_{min} and f_{max} must be

$$f_{max} \leq 1.4 f_{min}. \tag{4.1}$$

The center frequency and output frequency are chosen as following

$$f_c = \sqrt{f_{min} f_{max}}, \tag{4.2}$$

$$f_c \leq f_{out} \leq 1.05 f_c. \tag{4.3}$$

Although, our horn antenna has wideband applications. For such applications, the design specifications follow

$$1.4 f_{min} \leq f_{max} \leq 2.4 f_{min}, \tag{4.4}$$

$$f_c \approx 1.2 f_{min}, \tag{4.5}$$

$$1.05 f_c \leq f_{out} \leq 1.15 f_c. \tag{4.6}$$

However, after doing initial calculations, we found that the center frequency found following (4.5) lies in the upper end of the spectrum. Since we wanted a center frequency more towards the center of the spectrum, we follow (4.2) to give us a center frequency of 90 GHz.

4.1.2 Input and Output Radii

The input radius, a_i, is one of the main parameters of a horn as it decides the minimum size of the wave that can enter or exit through the antenna design. The fundamental mode of propagation in a circular waveguide is the TE_{11} mode. It's cut-off wave number is formulated as,

$$k = \frac{2\pi}{\lambda} = \frac{1.841}{a_i}. \tag{4.7}$$

This means, for the propagation of a wavelength corresponding to the minimum frequency of our design, the input radius must satisfy the following inequality where, c is the speed of light,

$$\frac{2\pi f_{min}}{c} a_i \geq 1.841. \tag{4.8}$$

This equation gives us a minimum value of a_i. Generally, a_i is chosen to be,

$$a_i = \frac{3\lambda_c}{2\pi}. \tag{4.9}$$

The Granet-paper [29], states that this choice of input radius ensures a return loss better than 15 dB at f_{min}.

The output radius, a_0, of a horn depends on the taper which is typically between -12 dB and -18 dB, and the beam width at which this taper is to be achieved. According to the Granet paper [29], the output radius should be chosen as depicted by Figure 4.1. However, as the 20 m dish has a very narrow half-subtended angle of 6.09°, a_0 is estimated to be between $4.8\lambda_c$ and $6\lambda_c$ depending on the taper profile used for the horn. We discuss profiles for the horn antenna in Section 4.1.4.

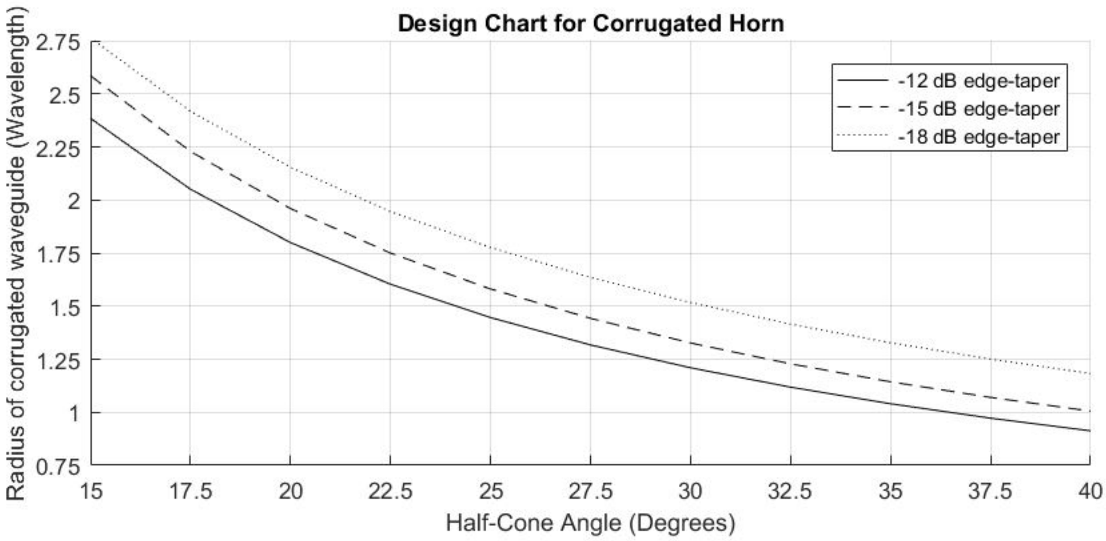

Figure 4.1: Estimation of output radius for a given taper and half-subtended angle according to the paper by Granet and James titled "Design of Corrugated Horns: A Primer" [29].

4.1.3 Length

The length, L, of a horn is determined by the application it is used for. A good initial starting point for most horns is $5\lambda_c$ to $10\lambda_c$. Due to our design being constrained by the half-subtended angle and taper requirements, we will require a much longer horn. The final value requires a lot of optimization and a good starting point for this design was between $30\lambda_c$ and $45\lambda_c$. The length of a horn effects the stability of its phase center as well as side-lobe levels.

4.1.4 Design Profiles

The profile of a horn affects radiation pattern shaping, side lobe levels and cross-polar levels. Profiling or shaping the curvature of the conical horn gives two major advantages in the design of a horn: control over mode conversion and shortening the device in length [30]. A lot of different types of profiles are available for smooth walled as well as corrugated horns. For simplicity, we mention only the profiles that were used in this project.

1. Exponential Profile

$$a(z) = a_i exp\left[ln\left(\frac{a_0}{a_i}\right)\frac{z}{L}\right] \tag{4.10}$$

2. Hyperbolic Profile

$$a(z) = \sqrt{a_i^2 + \frac{z^2(a_0^2 - a_i^2)}{L^2}} \tag{4.11}$$

3. Sinusoidal Profile

$$a(z) = a_i + (a_0 - a_i)\left[(1-A)\frac{z}{L} + Asin^{\rho}\left(\frac{\pi z}{2L}\right)\right] \tag{4.12}$$

4. xp Profile

$$a(z) = a_i + (a_0 - a_i)\left[(1-A)\frac{z}{L} + A\left(\frac{z}{L}\right)^{\rho}\right] \tag{4.13}$$

In sinusoidal as well as xp-profile, the design parameters ρ and A are defined. These are constants with A having a range between [0,1] and ρ generally having a value equal to 2, but has been found to give rise to interesting profile variations when varied between $0.5 \leq \rho \leq 5$.

4.2 Smooth Wall Horn Design Optimization

In Figure 4.2, a flowchart is presented for the design and optimization process of the smooth wall horn. This flowchart was repeated for all the four profile options mentioned in section 4.1.4. Since the main design work was carried out in CST, it was simple to parameterize the variables involved in the design process. Many optimization steps were involved to reach designs which satisfied our initial specifications. These are mentioned in sections 3.2, 3.3 and 3.6. In addition to these, a high radiation efficiency and gain are also important. Outer radius and length of the horn were the first parameters to undergo optimization. Initially, the optimization parameters were varied with large steps to investigate the variable search space (this involved a lot of iterations). When a promising candidate design was found, the step size was reduced to fine-tune the results towards the goal. For sinusoidal and xp profiles, additional optimization steps were used for ρ and A values. Changing these values changed the profile-shape of the horn and the results were interesting to analyze as they consisted of subtle but considerable changes in side-lobe levels. Again, initially a large step size was used and later a smaller step size was used to fine tune the results. Promising candidates were evaluated with the system assembly modelling (See Section 4.6) feature of CST to analyze the on-dish performance of the horn element in terms of aperture illumination.

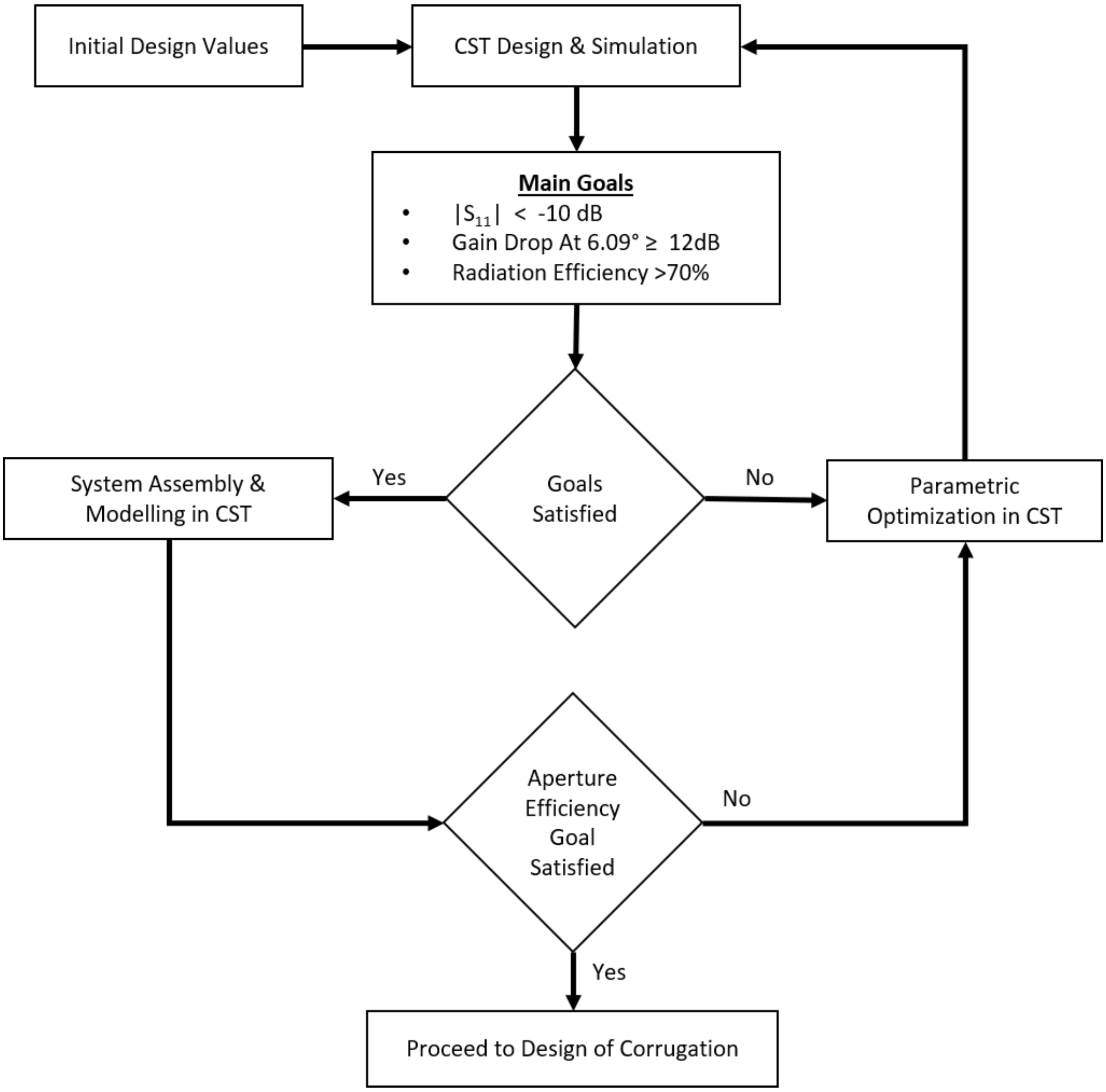

Figure 4.2: Optimization flowchart for the design of a smooth wall horn antenna.

4.3 Corrugated Horn

The design of corrugations is very important for good performance in a horn (See Section 2.6.1 to read more about corrugation theory). Corrugations consist of 'slots' which are empty rectangular spaces between 'teeth' like in a comb. The main parameters that need to be taken into consideration are slot pitch, slot width, slot pitch-to-width ratio, depth of the slots and design of the mode converter at the beginning of the horn. All the parameters are illustrated below for the understanding of the reader. As with the design mentioned in Section 4.1, the design procedure for corrugations mainly follows the paper by C.Granet and G.L.James [29]. Figure 4.3 shows a small section of corrugations with slots and teeth. Here, w is the slot width, d is the slot depth, p is the pitch or total length of a single corrugated segment. Each horn can be visualized as a collection of N segments of length p.

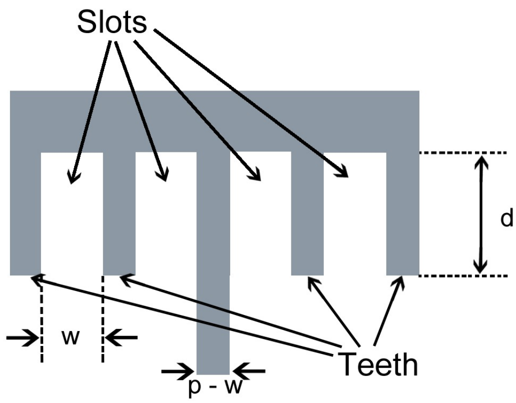

Figure 4.3: A section of the corrugations showing slots

4.3.1 Pitch

The pitch, p, of a slot is generally chosen to be between $\frac{\lambda_c}{10}$ and $\frac{\lambda_c}{5}$. In paper [29], it is noted that for broadband applications the pitch should be closer to $\frac{\lambda_c}{10}$ whereas for narrowband applications, the pitch should be closer to $\frac{\lambda_c}{5}$.

4.3.2 Slot Pitch-to-Width Ratio

The slot pitch-to-width ratio, δ, determines the width of the slot and the teeth. Generally, the slot width is larger than teeth width. It's value is usually between $0.7 \leq \delta \leq 0.9$.

4.3.3 Mode Converter

In the design of the corrugated horn for this project, we use a circular waveguide to attach the antenna to the feed receiver system. The first propagating mode (or fundamental mode) in a circular waveguide is the TE_{11} mode whereas the corrugated horn requires the propagation of hybrid HE_{11} mode. Hence, a mode converter segment is required at the beginning of the horn. The conversion happens over a number of slots in the converter. This value is denoted as N_{MC}, the number of corrugations in the mode converter as shown in Figure 4.4. In [29], three types of mode converters are presented,

1. variable-depth-slot mode converter for $f_{max} \leq 1.8 \leq f_{min}$,
2. ring-loaded-slot mode converter for $f_{max} \leq 2.4 \leq f_{min}$,
3. variable-pitch-to-width-slot mode converter for $f_{max} \leq 2.05 \leq f_{min}$.

Since our design specifications satisfy the condition for the variable-depth mode converter, we selected this design equation. More about ring-loaded-slot mode converter and variable-pitch-to-width slot mode converter can be read in [31] and [32]. The total number of slots, N_{MC} is between $5 \leq N_{MC} \leq 7$ for the variable depth mode converter, and the design equations are mentioned in section 4.3.4.

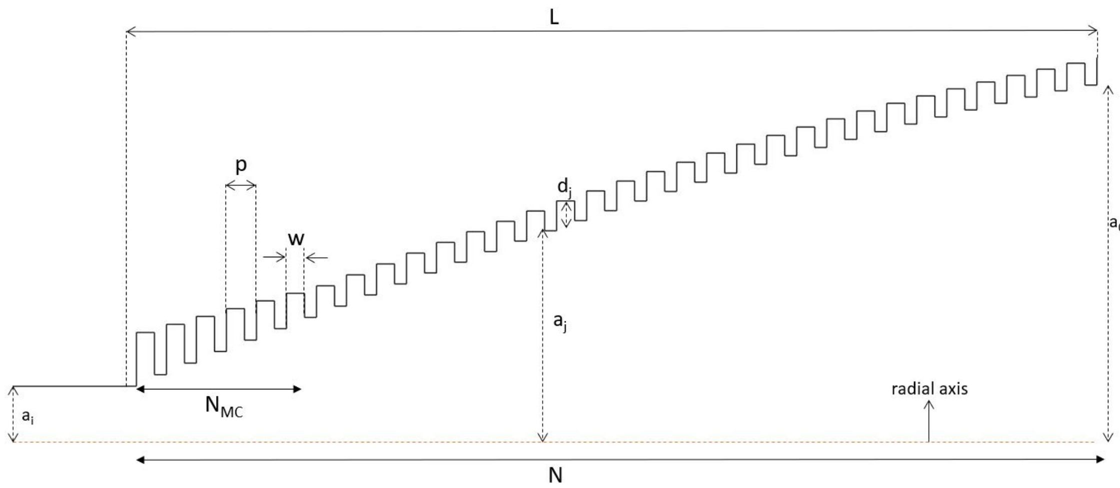

Figure 4.4: Basic geometry of a corrugated horn with variable-depth mode converter. The various parameters shown are input radius, a_i; output radius, a_0; length of the horn, L; corrugation pitch, p; slot width, w; slot depth of the j^{th} slot, d_j; number of corrugations in the mode converter, N_{MC}; total number of corrugations in the horn, N (this includes N_{MC}), and radius of the j^{th} corrugation, a_j.

4.3.4 Slot Depth Calculation

At any point along the horn with radius a_j and slot-depth d_j, the surface reactance of the corrugated surface is given by

$$\chi_j = -\delta \frac{J_1(k_c a_j)Y_1[k_c(a_j + d_j)] - Y_1(k_c a_j)J_1[k_c(a_j + d_j)]}{J_1'(k_c a_j)Y_1[k_c(a_j + d_j)] - Y_1'(k_c a_j)J_1[k_c(a_j + d_j)]} \tag{4.14}$$

where, $k_c = \frac{2\pi}{\lambda_c}$ is the wavenumber at center frequency f_c, J_1 is the Bessel function of the first kind of order one and $J_1^{'}$ is its derivative, similarly, Y_1 is the Bessel function of the second kind of order one and $Y_1^{'}$ is its derivative.
For hybrid modes to be balanced in the horn, we require $\| \chi_j \| \to \infty$. Hence, the denominator of (4.14) should be infinitesimally small or 0, which results in,

$$J_1^{'}(k_c a_j)Y_1[k_c(a_j + d_j)] - Y_1^{'}(k_c a_j)J_1[k_c(a_j + d_j)] = 0. \tag{4.15}$$

Nominally, for this condition to be satisfied, the value of d_j is set to $\frac{\lambda_c}{4}$, according to [29] however, a correction factor κ obtained from the solution of (5.2) can be multiplied with the nominal value of d_j to give better performance results. The value of κ was approximated as

$$\kappa = exp\left[\frac{1}{2.114(k_c a_j)^{1.134}}\right] \tag{4.16}$$

The equations for the calculation of slot depths for the mode converter and the horn are as follows:
For slots up to N_{MC}+1,

$$d_j = \left[\sigma - \frac{j-1}{N_{MC}}\left(\sigma - \frac{1}{4}exp\left[\frac{1}{2.114(k_c a_j)^{1.134}}\right]\right)\right]\lambda_c \tag{4.17}$$

where, σ is the percentage factor for the first slot depth of the mode converter and varies as $0.4 \leq \sigma \leq 0.5$.
For the rest of the corrugations, the depth of the jth slot is equated as,

$$d_j = \frac{\lambda_c}{4} exp\left[\frac{1}{2.114(k_c a_j)^{1.134}}\right] - \left(\frac{j - N_{MC} - 1}{N - N_{MC} - 1}\right)\left(\frac{\lambda_c}{4} exp\left[\frac{1}{2.114(k_c a_0)^{1.134}}\right] - \frac{\lambda_{out}}{4} exp\left[\frac{1}{2.114(k_{out} a_0)^{1.134}}\right]\right) \quad (4.18)$$

Note that the output frequency f_{out} and corresponding wavelength λ_{out} have been used in the latter part of this equation for calculation of slot depths.

4.4 Corrugated Horn Design Optimization

Figure 4.5 shows the optimization procedure followed for achieving the design specifications for the corrugated horn. The design process starts with promising models from the smooth wall horn optimization, this way we have already filtered out many (hundreds) incompatible horn designs. The parameters and corrugated profile was created in MATLAB. The file was then exported to CST and added as a 3-D curve which was then modelled into the full circular corrugated horn. The simulation process was again carried out in CST and results were analyzed. Corrugation design has a large number of variable parameters that need to be optimized, unfortunately due to time constraints, only a handful parameters were manipulated to give a desirable horn design. Optimization was performed on MATLAB by changing parameters to get favourable results in terms of S-parameters, gain, beam-width as well as aperture efficiency. One could argue that an optimization algorithms like evolutionary algorithm could be used, but again, due to the aforementioned time constraint, these techniques would have taken longer to study and implement. Fortunately, since we had narrowed down the compatible smooth horn candidates down to 3 cases, this simplified optimization scheme gave us a good horn design for our specifications.

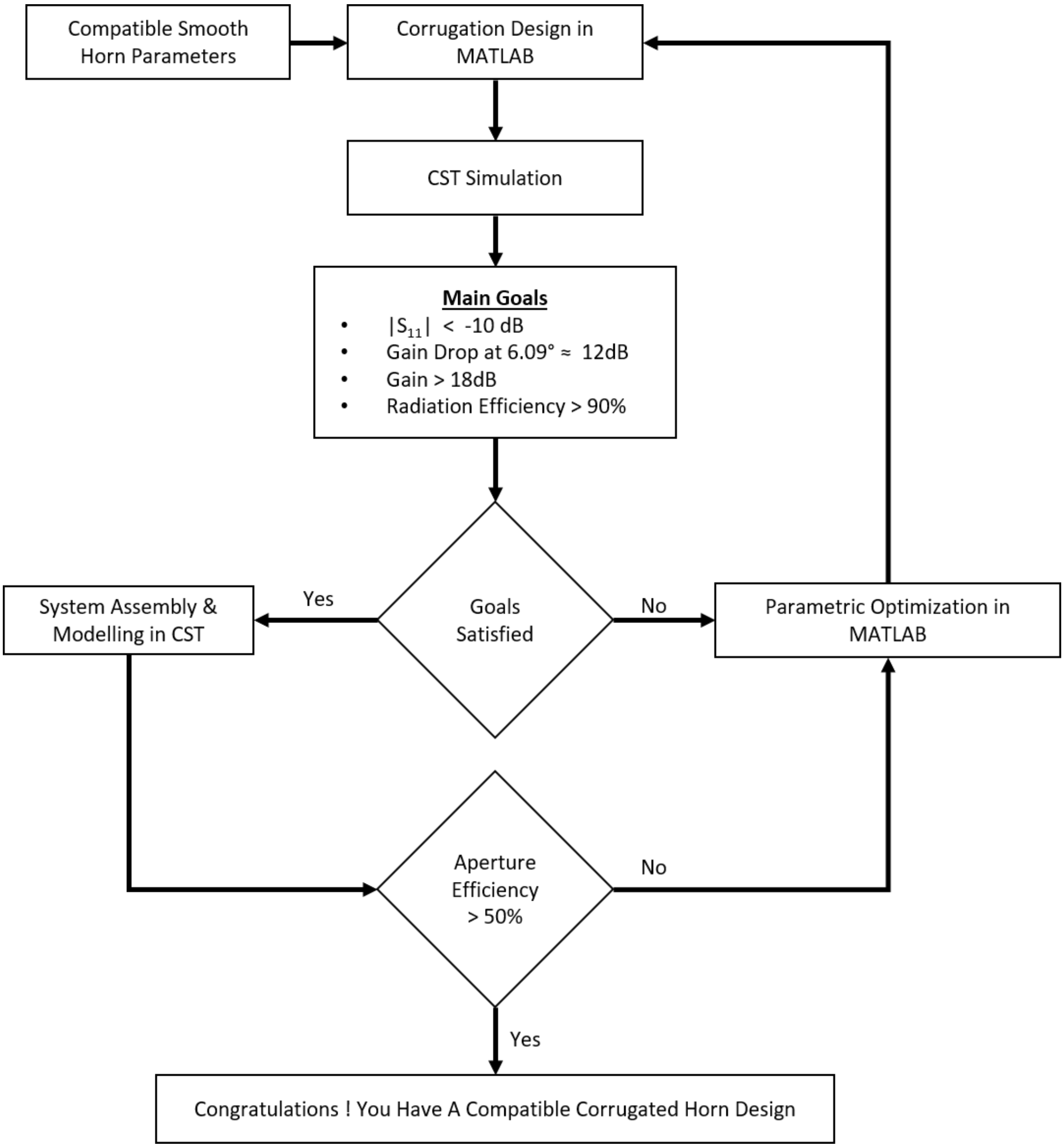

Figure 4.5: Optimization flowchart for the design of a corrugated horn antenna.

4.5 System Assembly and Modelling

System Assembly and Modelling (SAM) is a powerful evaluation tool that was added on to CST Microwave Studio's 2014 edition. SAM allows users to take a component and check its performance combined with another component. At the component level, designs are performed independent of a complete system model. Designers often ignore the interdependence of individual components at the system level. In SAM this interdependence can be tested and analyzed. The environment consists of a lot of different applications including simulation of thermal coupling, far field analysis of a feed element on a larger dish, electromagnetic analysis of various components etc [33], [34].

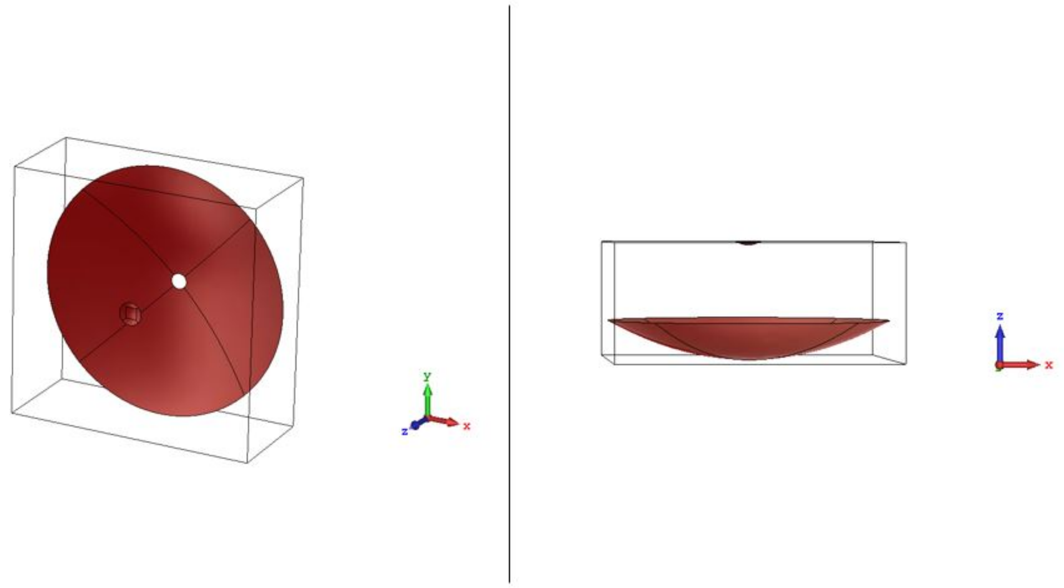

Figure 4.6: 20 m dish model used for asymptotic analysis in the SAM environment.

The SAM environment also gives the option of using different types of solvers such as time domain solver, frequency domain solver, asymptotic solver, eigenmode solver, integral equation solver and multilayer solver. In the analysis of this design, we use an asymptotic solver [35]. This type of solver uses the Shooting Bouncing Ray (SBR) method which is an extension of physical optics (PO). This method was initially developed for radar cross section analysis but can also be used for analysis of feed performance on the main dish like in the case of this project. In the shooting bouncing ray method, rays, following the laws of geometrical optics (GO) bounce around the cavity walls and eventually exit the cavity via the aperture.
In this project, a file containing the 20 m dish model was provided by Jonas Flygare. Wideband far field sources were imported from candidate horn designs and an asymptotic analysis was used to see how a single feed performs on the 20 m dish. This analysis shows how much of the dish was illuminated by the horn feed. Using the resulting telescope far field gains, aperture efficiency as mentioned in section 2.1.7 was calculated through MATLAB.

5
Results and Discussion

This chapter displays and discusses the results obtained through this project. We discuss the initial parameters that were set and change, if any, in those parameters, followed by results of S-parameters, far field patterns and aperture efficiency for smooth wall horn and corrugated horn. Results for sensitivity are presented at the end of the chapter for the corrugated horn design only.

5.1 Smooth Wall Horn

Following the design process mentioned in Chapter 4, initial parameters were calculated as given in Table 5.1. These were the starting parameters used for all designs. The initial smooth wall horn design was optimized to find suitable candidates for corrugated horn design.

Quantity	Symbol	Value
Minimum Frequency	f_{min}	70 GHz
Maximum Frequency	f_{max}	116 GHz
Center Frequency	f_c	90 GHz
Output Frequency	f_{out}	99 GHz
Center Wavelength	λ_c	3.331 mm
Output Wavelength	λ_{out}	3.028 mm
Inner Radius	a_i	1.59 mm
Outer Radius	a_0	14.16 mm
Length	L	83.275 mm

Table 5.1: Initial parameter values for all profile design.

The inner radius according to (4.9) was initially calculated as 1.704 mm. A better choice was to use an existing standard circular waveguide for simplicity and cost efficiency in the manufacturing process. Hence, a standard waveguide produced by Cernex [36] for the E-band with a diameter of 3.18 mm was chosen. This was so that the wavelength of the smallest frequency could enter the waveguide. Figures 5.1 – 5.4 show the smooth wall horn design as done in CST. In each image, part (a) shows a cutting plane view where the shape of the profile is seen and part (b) shows the full horn element. We can see the difference in the shape of each profile. As mentioned in Section 4.1.4, profiling the element helps to shorten the device length and gives control over mode conversion. In the design, an extra cylindrical segment is added to the beginning of the design in order for the electromagnetic solver of CST to mesh the structure properly, and excite mode propagation.

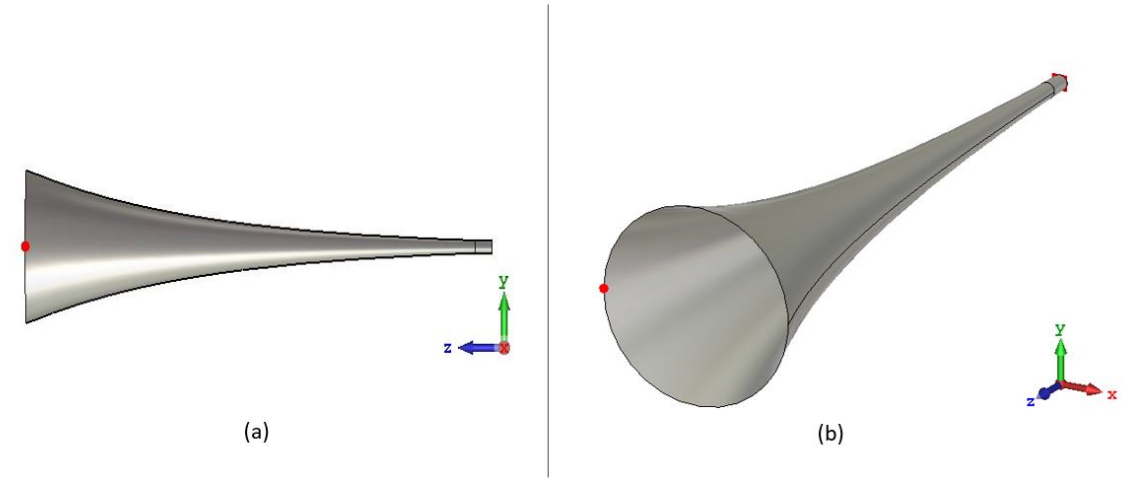

Figure 5.1: Smooth wall horn with exponential profile.

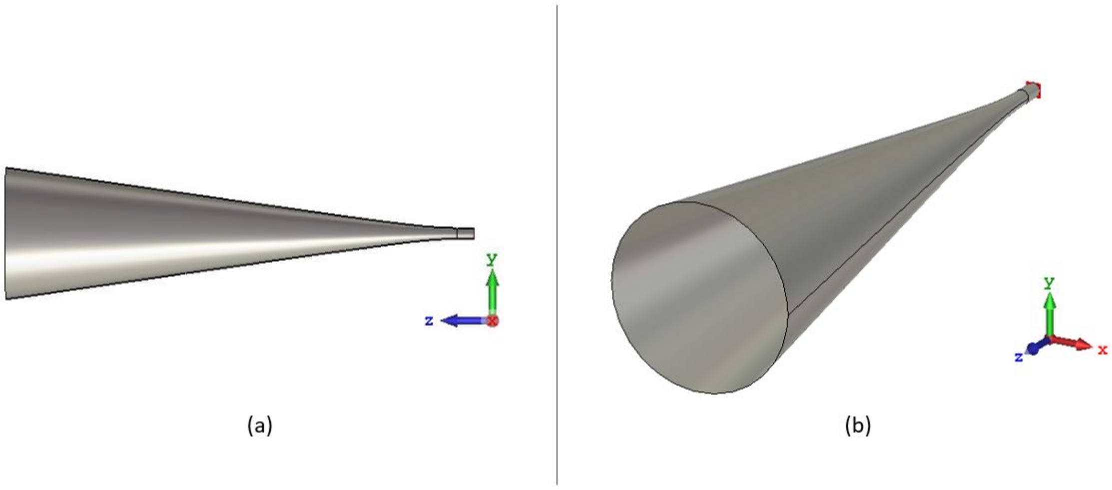

Figure 5.2: Smooth wall horn with hyperbolic profile.

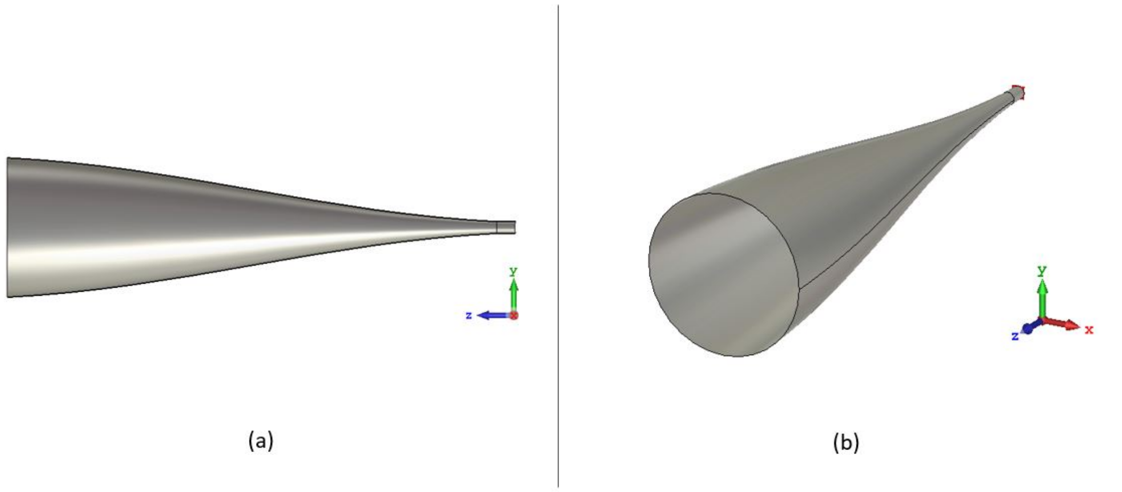

Figure 5.3: Smooth wall horn with sinusoidal profile.

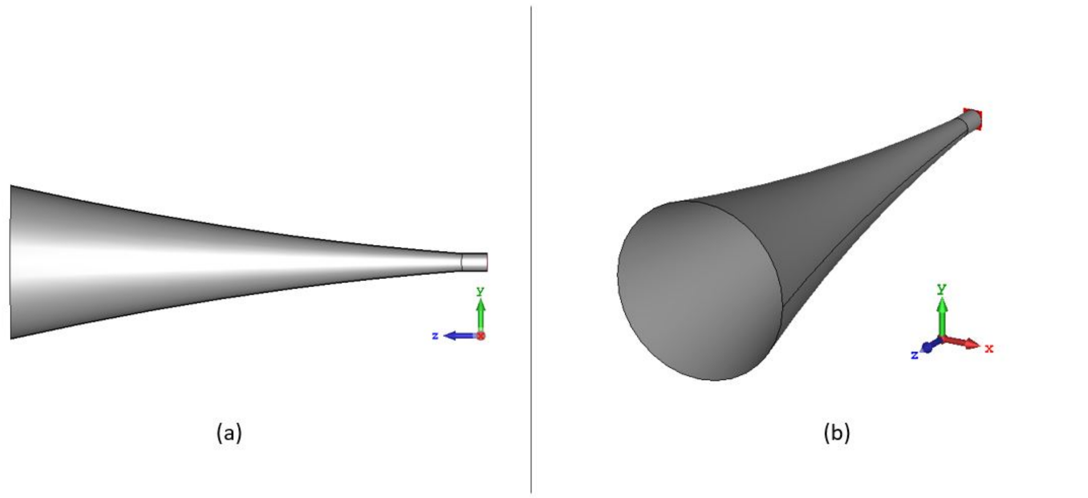

Figure 5.4: Smooth wall horn with xp profile.

Optimization of the smooth horn design for the exponential and hyperbolic profiles, was performed for outer radius, a_0 and horn length, L. Sinusoidal and xp profiles also included optimization of design parameters A and ρ (4.12) and (4.13). Since the design was specifically for a very narrow beam width, parametric optimization was done in two steps. First, the parameter sweep was performed with a large step size (specifically to length and outer radius) to see which range could provide us with suitable results. Second, the step size was reduced to fine-tune promising candidate designs to achieve S11 < -10 dB, as presented in Figure 4.2. Often a third step was involved to further fine tune the design and obtain more specific values. The optimization was time-consuming due to long iteration time (around 10 minutes per iteration per profile) for all the four profiles. To limit the size of this report, we will go through the final results from the smooth wall horn design.

5.1.1 Exponential Profile

Smooth wall horn design in the exponential profile resulted in a low reflection coefficient S_{11} < -22 dB and a gain ranging between 20 dBi and 28 dBi. However, the beam width achieved through this design was broad and failed to meet our specifications. The length was parametrized and varied up to $50\lambda_c$, however results from $45\lambda_c$ showed poor performance in the horn, affecting its radiation efficiency as well as cross-polarization levels. The outer aperture was also varied, but the length of the horn was the major constraint in this design to achieve the specified beamwidth. Hence, we do not consider the exponential profile for the design of the horn any further.

5.1.2 Hyperbolic Profile

Hyperbolic profile provided results similar to the exponential profile. Reflection coefficient levels were better than S_{11} < -30 dB for most iterations. Gain of the design varied between 20 dBi and 28 dBi. However, like in the case of the exponential horn, the beamwidth requirements were failed to be met by this profile design and the length of horn, L > $45\lambda_c$ made the horn performance very poor. This profile was also disqualified and not considered for further evaluation.

5.1.3 xp Profile

The xp profile achieved slightly different results in terms of gain as compared to all the other profiles. The input reflection-coefficient values were at an average of -25 dB for most iterations and the gain varied between 18 dBi and 25 dBi. Again, the horn performance became very poor at lengths exceeding $45\lambda_c$. On variation of its profile design parameters A and ρ, some of the iterations achieved the specified beamwidth and were taken forward to the corrugations design process, but did not meet the specifications after that stage.

5.1.4 Sinusoidal Profile

Sinusoidal profile provided very good results in terms of reflection coefficient, gain as well as beamwidth requirement. Due to the specified of the beamwidth being extremely narrow, we chose designs which gave a gain drop as close to 12 dB as possible. As in the case of all other profiles, in designs with horn length exceeding $45\lambda_c$, the horn produced very poor values of radiation efficiency. Two possible sinusoidal profiles were selected and taken forward to the corrugated horn design. However, for simplicity, we will only go through and discuss the results of the design whose parameters were used for the final corrugated horn.

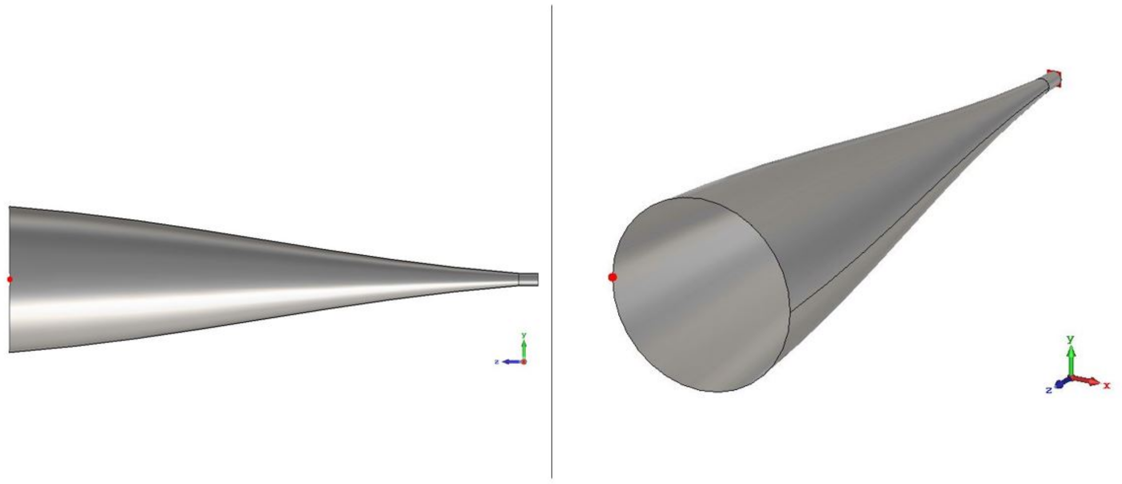

Figure 5.5: Smooth wall sinusoidal horn design for the specification in Table 5.2.

5.2 Smooth Horn Results

The dimensions of the smooth horn sinusoidal profile design results discussed in this section are given in Table 5.2, and the design is presented in Figure 5.5. We observe that the outer aperture is much larger than the input aperture, this is due to our specification for having a very narrow beamwidth and edge taper.

Quantity	Symbol	Value
Center Wavelength	λ_c	3.331 mm
Inner Radius	a_i	1.59 mm
Outer Radius	a_0	18.99 mm
Length	L	133.24 mm
Profile Design Parameter	A	0.4
Profile Design Parameter	ρ	2

Table 5.2: Smooth horn sinusoidal profile design parameters.

5.2.1 Reflection Coefficient

Figure 5.6 shows the input reflection coefficient for the designed smooth horn. As observed it is well below our requirement of S_{11} < -10 dB. Throughout the band, it is below S_{11} < -25 dB. This means that there is an extremely small reflection loss of 0.3% at the input of the horn feed.

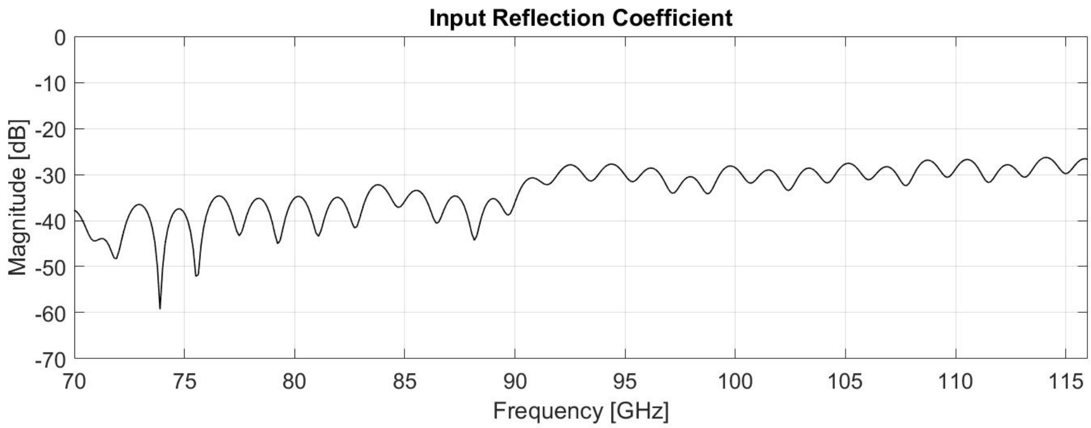

Figure 5.6: Simulated input reflection coefficient, S_{11}, for the smooth wall horn design.

5.2.2 Radiation Efficiency

Radiation efficiency of an antenna shows how well the antenna converts the radio power accepted at the terminals into radiated power. A high value of radiation efficiency is essential for good electrical performance of an antenna. In our design, the radiation efficiency varies from a maximum of 99.5% at 75 GHz to a minimum of 83.2% at 116 GHz. We also observe that as the frequency increases, the radiation efficiency decreases as is the standard trend [37]. The expectation is that the radiation efficiency will become better when the wall of the horn is corrugated

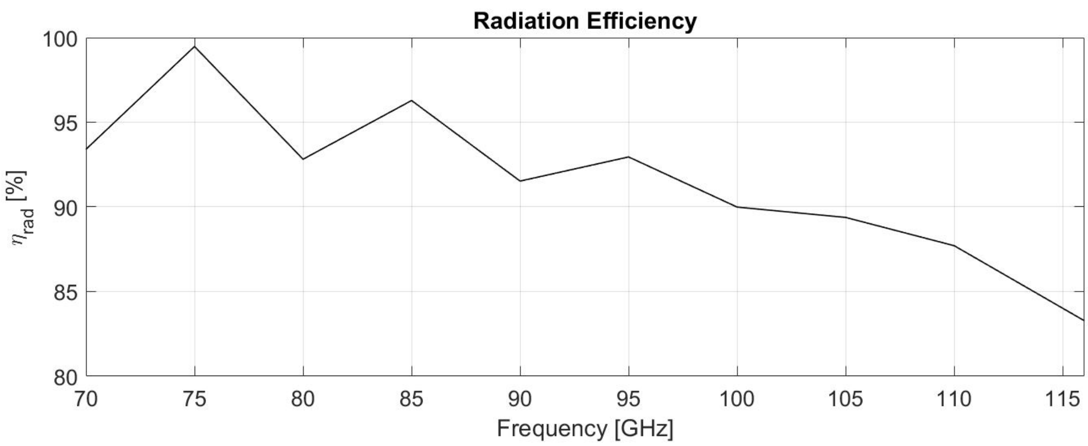

Figure 5.7: Simulated radiation efficiency for the smooth wall horn design.

5.2.3 Aperture Efficiency

Figure 5.8 shows the simulated aperture efficiency, η_a, of the smooth wall horn design, on the Onsala 20 m dish. The aperture efficiency is simulated using the SAM technique in CST (See Section 4.6). For the smooth wall horn, η_a is close to 50% across the band. Aperture efficiency depends on the phase center placement of the feed element in the parabolic dish. Ideally, for optimal phase efficiency, the feed should be placed such that the reflector focal point coincides with the phase center. Over a wideband, the phase centers of the frequencies should averagely be around the same distance. For this thesis, the feed phase centre was calculated as the average of phase centers over the frequency band and the feed was kept at a constant location for the calculation over the whole band. The location of the feed must be close to the focus of the dish at 100 GHz which could explain the slight elevation of η_A around 100 GHz.

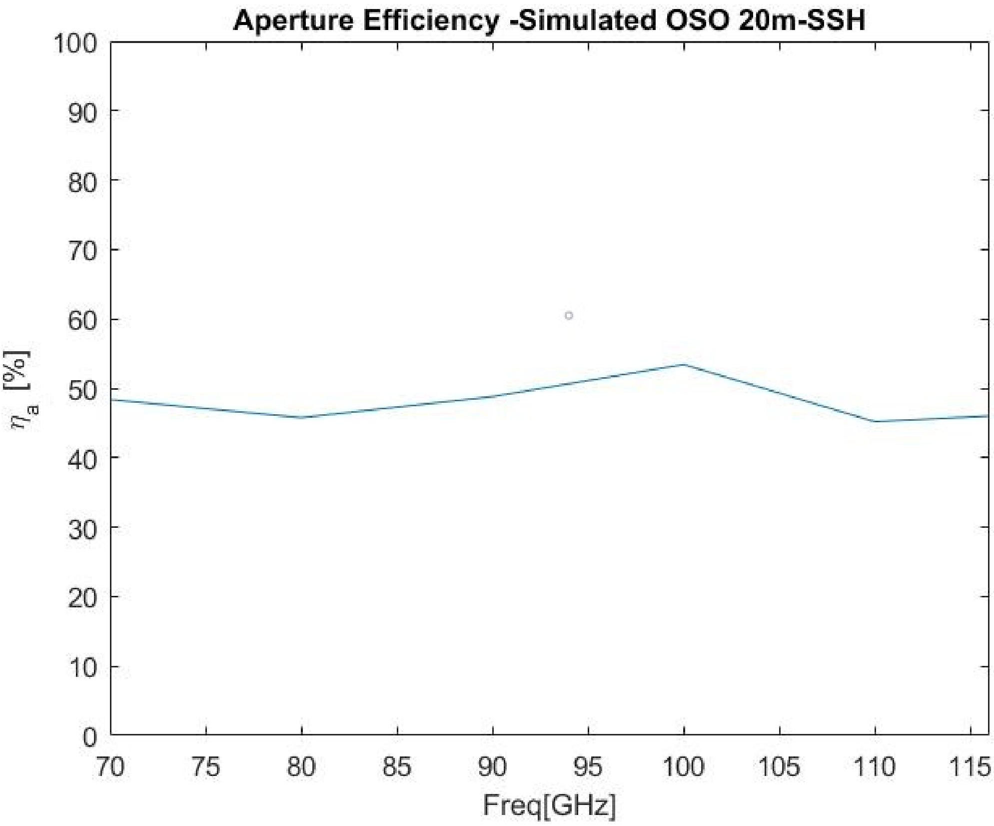

Figure 5.8: Aperture efficiency, η_A, in percentage, for the smooth wall horn design. The aperture efficiency is seen to be at an average of 50%, peaking at 100 GHz to 53.44%.

5.2.4 Beam Patterns

Farfield beam patterns for the smooth wall horn design have been given in figures 5.10 – 5.12. The beam patterns have been normalized with maximum gain in each case. The figures compare farfields at three different frequencies (70 GHz, 90 GHz and 116 GHz) at three different ϕ-planes (ϕ = 0°or E-Plane, ϕ=45°or D-Plane and ϕ = 90°or H-Plane). Each image shows the co-polarization as well as the cross-polarization pattern, in Ludwig's 3rd definition. In E-plane and H-plane the cross-polarization pattern cannot be seen in the images as it is below -80 dB. In the D-plane the cross-polarization level relative to maximum gain, for: 70 GHz, is -17 dB; 90 GHz, is -14.9 dB and 116 GHz, is -12.6 dB. Corrugated horns generally have a low cross-polarization level, so we expect to see better cross- polarization levels in the results of the corrugated horn design.

Figure 5.9 shows the gain drop at θ = 6.09°which was required to be approximately -12 dB. This specification was set so that the taper level matches that of the parabolic reflector to lessen the spillover loss. Since it is very difficult to achieve this taper value for a beam as narrow as in our project, we settle for a value closest to -12 dB at 90 GHz in the E-Plane, in this case, the gain drops -11.713 dB at θ = 6.09°.

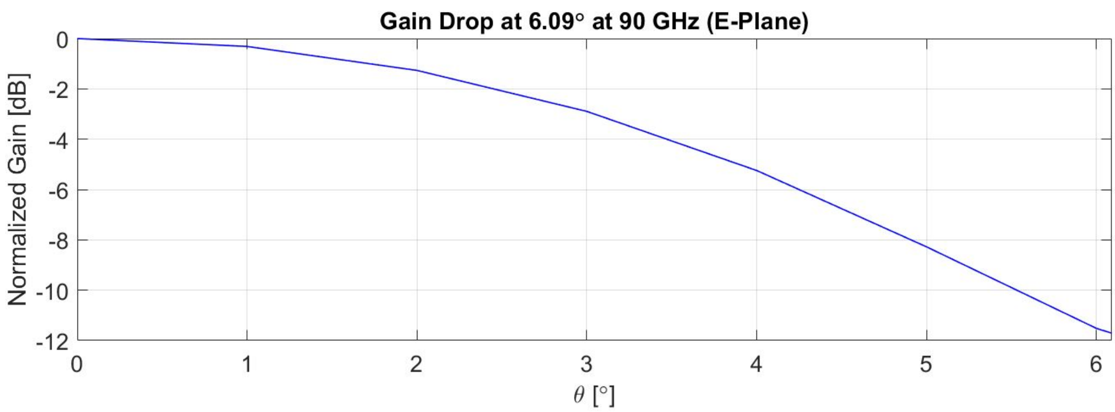

Figure 5.9: Gain drop at θ=6.09°at 90 GHz in the E-Plane, is seen to be 11.713 dB for the smooth horn design.

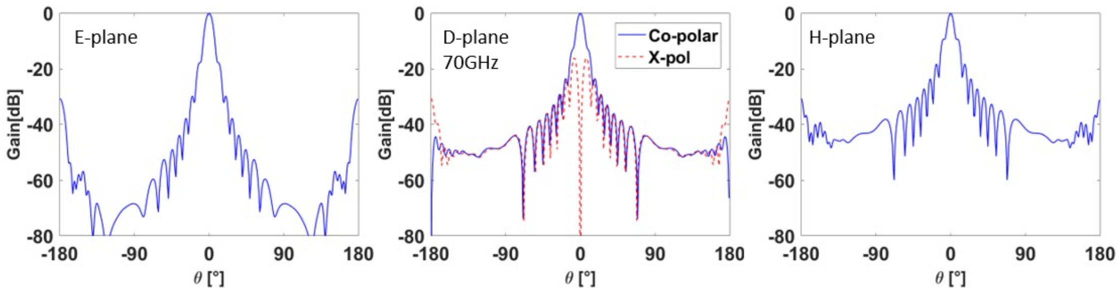

Figure 5.10: Simulated farfield beam patterns at 70 GHz in E-, D- and H-Plane for the smooth wall horn antenna design.

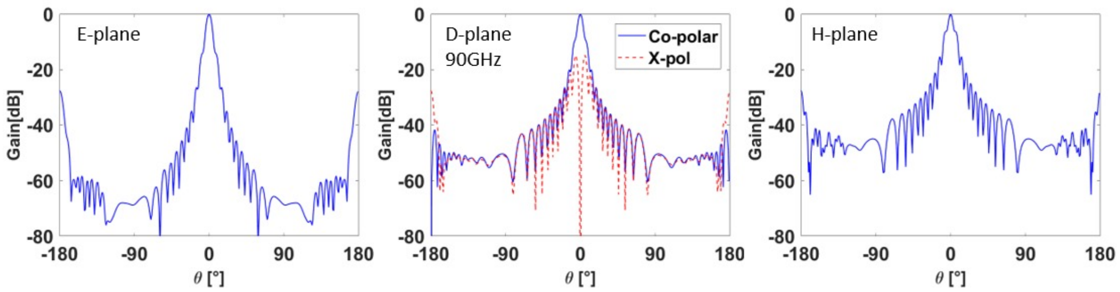

Figure 5.11: Simulated farfield beam patterns at 90 GHz in E-, D- and H-Plane for the smooth wall horn antenna design.

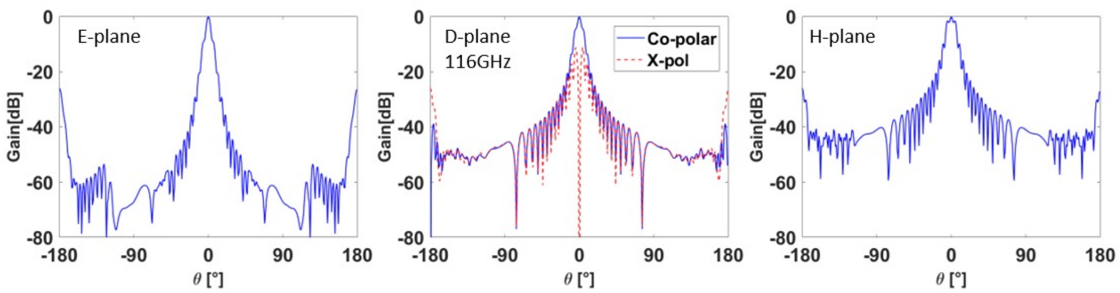

Figure 5.12: Simulated farfield beam patterns at 116 GHz in E-, D- and H-Plane for the smooth wall horn antenna design.

5.3 Corrugated Horn

Corrugation geometry for the horn was designed in MATLAB according to the equations given in Chapter 4. To get the stepped geometry in the horn, the corrugations were set as $2N$ (N being the total number of corrugations) circular sections of finite length arranged one after another (the teeth and slots alternating). The resulting design is shown in Figure 5.13. Design parameters of the final corrugated horn design are presented in Table 5.3.

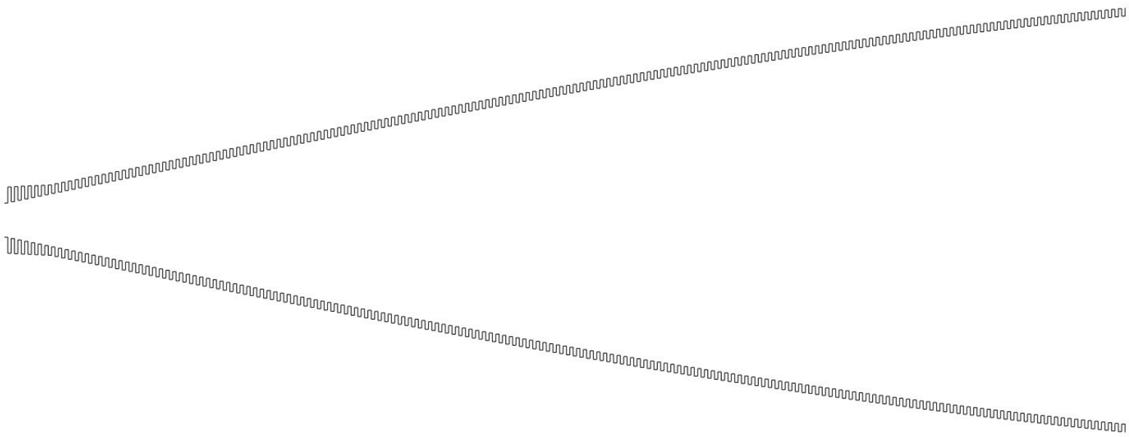

Figure 5.13: The stepped corrugation geometry for the final corrugated horn design as created in MATLAB.

Quantity	Symbol	Value
Minimum Frequency	f_{min}	70 GHz
Maximum Frequency	f_{max}	116 GHz
Center Frequency	f_c	90 GHz
Output Frequency	f_{out}	99 GHz
Center Wavelength	λ_c	3.331 mm
Output Wavelength	λ_{out}	3.028 mm
Inner Radius	a_i	1.59 mm
Outer Radius	a_0	19.75 mm
Length	L	133.64 mm
Slot Pitch	p	0.8 mm
Pitch-to-width ratio	δ	0.5
Total no. of corrugations	N	167
No. of corrugations in mode converter	N_{MC}	6

Table 5.3: Final corrugated horn design values.

The approach for designing the corrugations was taken from the paper by Granet and James [29], however some variations were made to make the design easier for manufacturing. The paper suggests that the pitch be chosen such that

$$\frac{\lambda_c}{10} \leq p \leq \frac{\lambda_c}{5}$$

with wide-band horns having a pitch closer to $\frac{\lambda_c}{10}$. This means that for our chosen center frequency and horn length, we would require about 400 corrugations which gives us a slot width of 0.165 mm for our selected slot-to-width ratio. In practical terms this means a very costly horn design with a very complex manufacturing procedure. Hence to reduce the cost and complexity of the horn we selected a pitch which was approximately $\frac{\lambda_c}{4}$. This leads us to having 167 corrugations that gives us roughly 3 corrugations per wavelength. This is the minimum number of corrugations per wavelength required as per [25] . Another parameter that was chosen differently is the slot pitch-to-width ratio, δ. The Granet-paper [29], suggests that the the value of δ be,

$$0.7 \leq \delta \leq 0.9,$$

but when tested, these values gave very high cross-polarization levels. Upon further research, it was found that for high frequency wide-band horns, it is better to have equal widths for slots and teeth which gives us, $\delta = 0.5$ [25]. This selection of pitch meets with our specifications of cross polarization levels. The corrugation geometry mainly affects the cross polarization levels in a horn, as discussed below. Figure 5.14 shows the simulated corrugated horn geometry as designed in CST Microwave Studio, the picture on the top shows a cutting plane section whereas the picture on the bottom shows the full horn design as well as designed boundaries. The red rectangular patch in the bottom picture shows the waveguide port where the horn is excited.

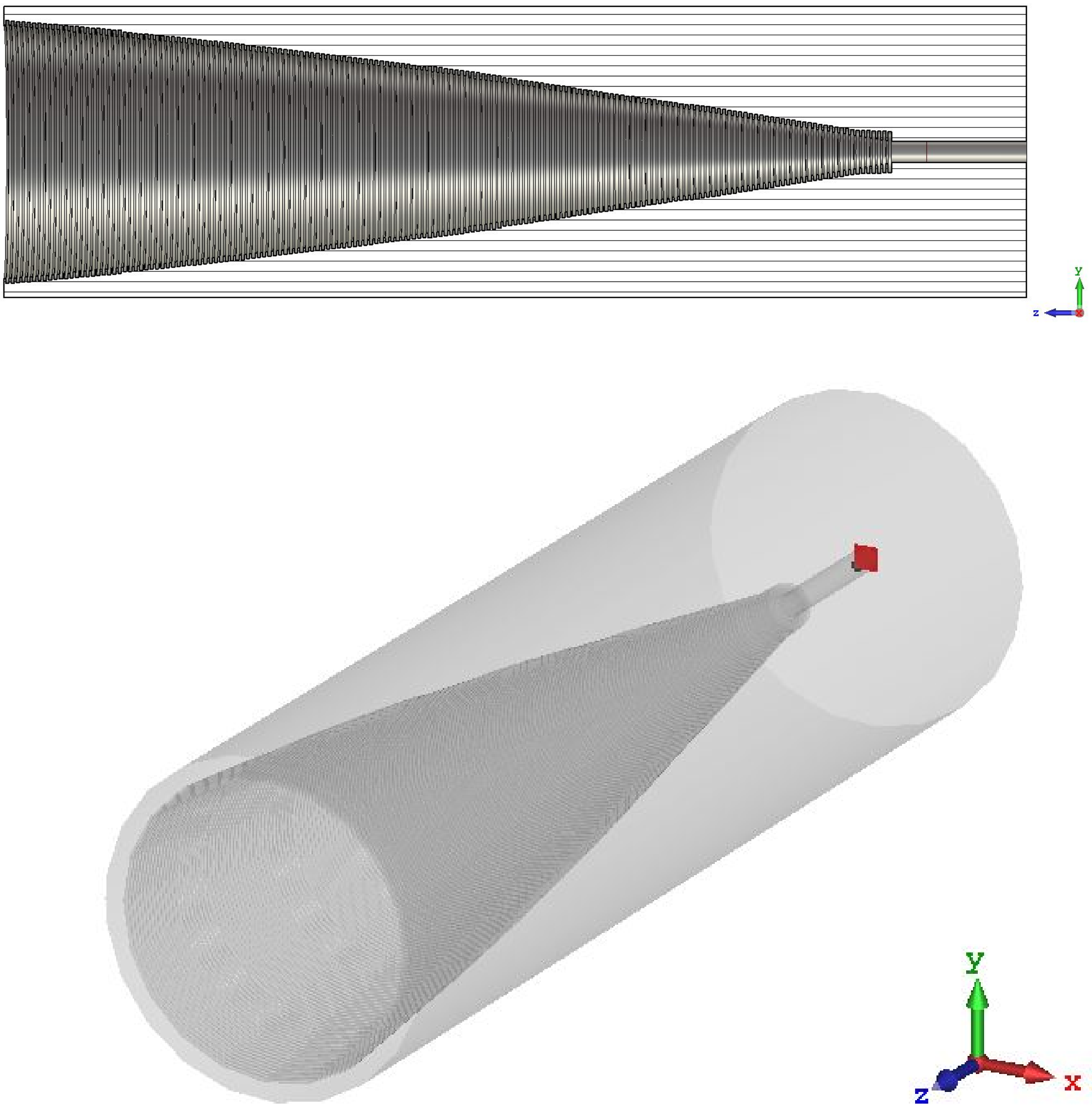

Figure 5.14: The corrugated horn as designed in CST Microwave Studio. The image on the top shows a cutting plane cross-section of the horn whereas the picture on the bottom shows the full circular design. The red rectangular patch on the bottom image shows the waveguide port which is used for the excitation of the horn.

5.3.1 Reflection Coefficient

Figure 5.15 shows the simulated input reflection coefficient over the band for the corrugated horn design. Over most of the band, the reflection co-efficient is well below -22 dB, however at the beginning of the spectrum for 70 GHz, the reflection coefficient is approximately -18 dB. This shows that there is potential mode mismatch at the throat of the horn, which means the transition from TE_{11} mode to

HE_{11} mode is not smooth and efficient. This suggests that the mode converter might need a better design in order to have low reflection coefficient like over the rest of the band. This value of S_{11} meets our specification of having an input reflection coefficient better than S_{11} < -10 dB and hence is accepted as a good range over the band.

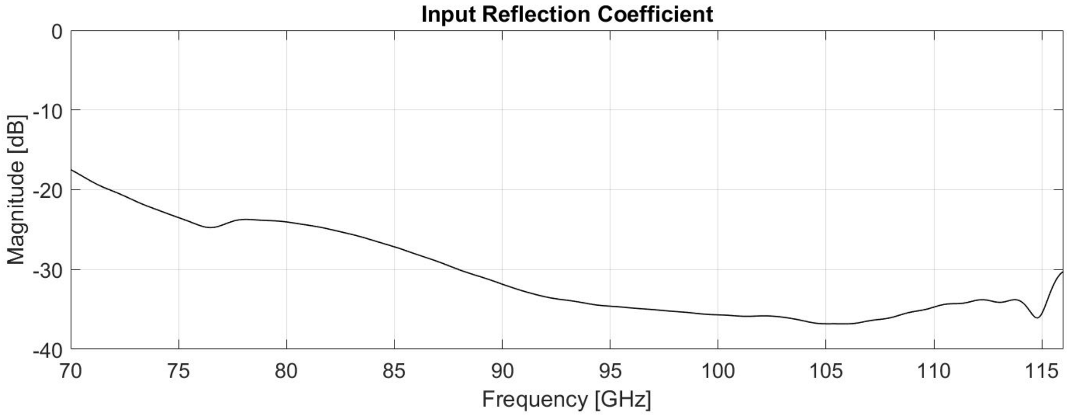

Figure 5.15: Simulated input reflection coefficient for the final corrugated horn design. The relatively high value at the beginning of the spectrum suggests that there might be mode mismatch in the mode converter region of the horn.

5.3.2 Radiation Efficiency

The radiation efficiency of the corrugated horn, as shown in Figure 5.16, is over our required specification of 90% (better than 95%) over the band. The relatively lower value for the band between 70 and 80 GHz again suggests that there might be some defect in the transition region but also goes to show that the defect is not a very large one as it still provides a very efficient horn. Simulating the radiation efficiency of a low-loss antenna with good accuracy is hard [38]. Our result indicates that the value is quite high which is expected and hence, good enough for this thesis.

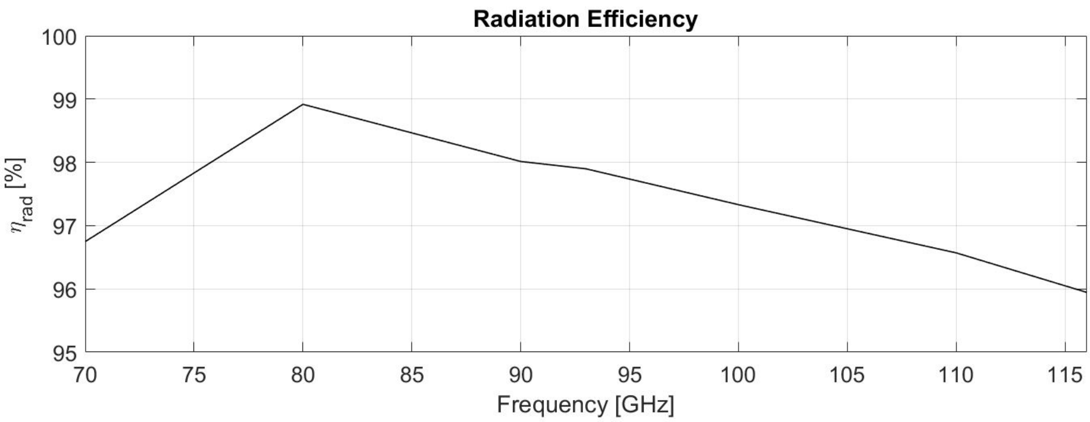

Figure 5.16: Simulated radiation efficiency for the corrugated horn design. The radiation efficiency over the whole band is better than 95% which meets our required specifications

5.3.3 Aperture Efficiency

Simulated aperture efficiency of the horn is shown in figure 5.17. Over the band, $\eta_A > 60\%$ and averages at about 65% with a peak of 69.67% at 110 GHz. This is a good value for corrugated horns and is well over our minimum requirement of $\eta_A > 50\%$. Perhaps, if the mode mismatch is corrected, the efficiency will be higher. Of course, η_A is also affected as there is spillover loss due to the beamwidth not being narrow enough (see the next section for results). As in the case of the smooth horn design, the phase center for the corrugated horn feed was taken as the average value of phase centers over the band. The feed was kept at a constant location throughout the SAM analysis.

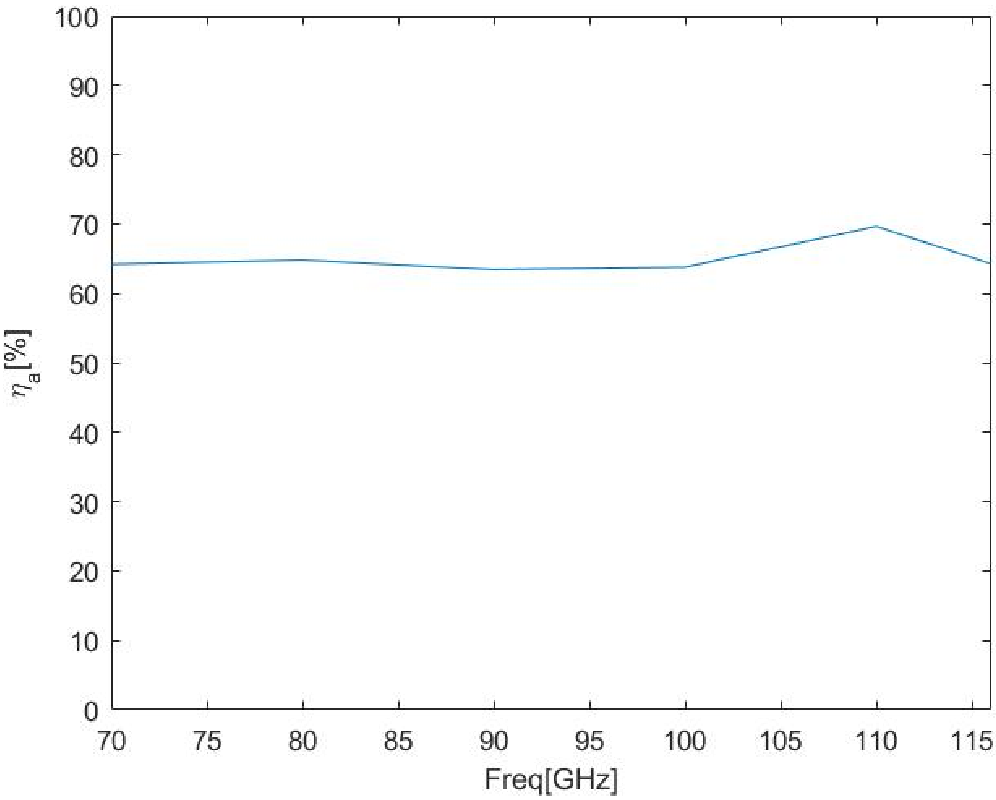

Figure 5.17: Aperture Efficiency, η_A, in percentage, for the corrugated horn design. The aperture efficiency is seen to be at an average of 65%, peaking at 110 GHz to 69.67%

5.3.4 Beam Patterns

Figure 5.18 shows the gain drop of the corrugated horn design at 6.09°. The drop in this case is -11.356 dB which is less than our requirement of -12 dB. This suggests that the aperture of the corrugated horn needs to be optimized to get the required -12 dB taper required for the small half-subtended angle of the 20 m dish. A broader feed beamwidth means that there is more spillover loss which affects the aperture illumination efficiency and sensitivity of a parabolic reflector.

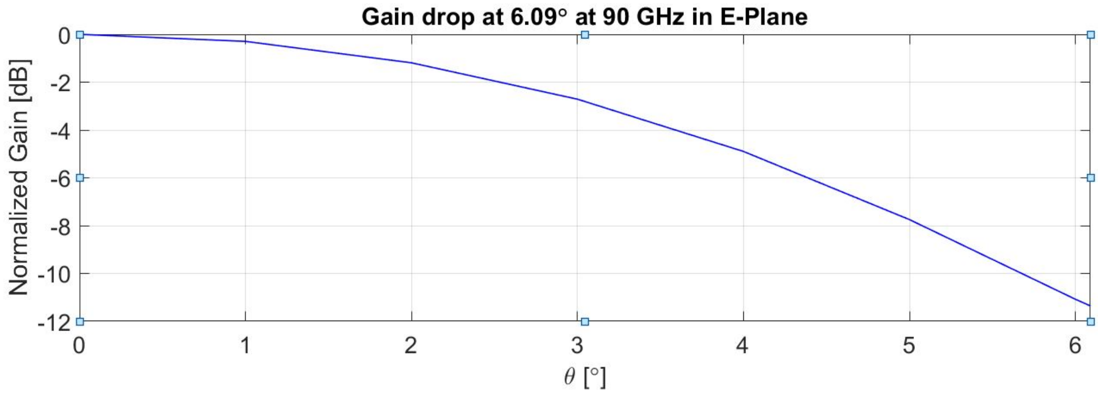

Figure 5.18: Gain drop at θ=6.09°at 90 GHz in the E-plane, is seen to be 11.356 dB for the corrugated horn design.

Figures 5.22, 5.23 and 5.24 show the simulated beam patterns of the corrugated horn at farfield. The beam patterns are shown for three different frequencies (70 GHz, 90 GHz and 116 GHz) in three different planes (ϕ=0 or E-plane, ϕ=45 or D-plane and ϕ=90 or H-plane). Each image shows the co-polar and cross-polar component of the pattern and we observe that the cross-polarization pattern for the E-plane and H-plane is extremely low (> -100 dB) and hence cannot be seen in the images. The cross-polar pattern can be seen in the D-plane as it has the worst performance in this plane. Corrugated horns have very low cross-polarization levels relative to the maximum gain of the horn, this is one of the main reasons that they are used as feeds for parabolic reflectors. In our design, we can calculate the cross-polarization level relative to the maximum gain for the ϕ = 45°plane at 70, 90 and 116 GHz. The levels are tabulated in Table 5.4 below. Figure 5.19 shows the cross-polarization levels relative to maximum gain in the D-plane over the frequency band.

Frequency [GHz]	Cross-Polarization Level [dB]
70	-37.6
90	-35.2
116	-19.5

Table 5.4: Cross-Polarization levels relative to the maximum gain for the corrugated horn design, in D-Plane.

The cross-polarization peak values for the 70 GHz and 116 GHz frequencies at

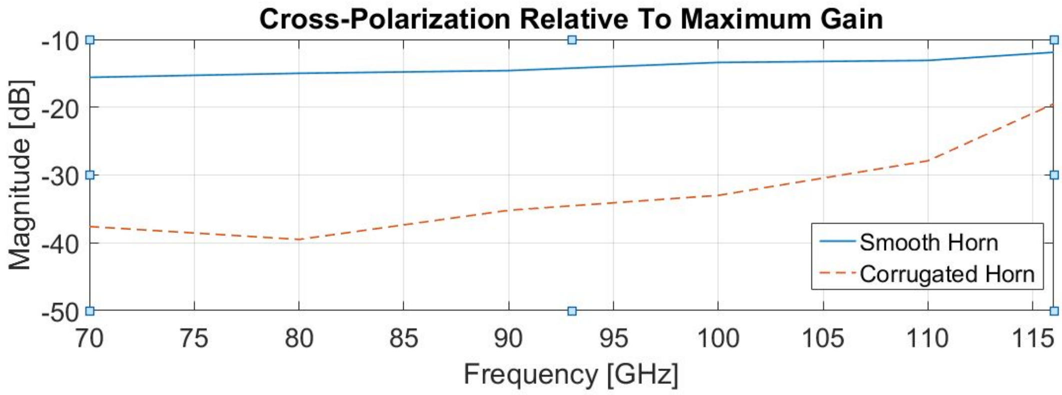

Figure 5.19: Cross-polarization levels relative to the maximum gain in the D-Plane for the smooth horn design and corrugated horn design over the frequency band.

θ=90°, whereas for 90 GHz, the cross-polarization peak lies at θ=180°. This could also be due to the mode mismatch at the input of the horn, due to the mismatch more power is pushed into the back lobes of the antenna causing the cross-polarization to peak in the region. Generally, cross-polarization levels below -10 dB are considered good enough for single mode performance. Comparatively, our results are very good.

Another characteristic of the corrugated horn antenna is beam symmetry. Figure 5.20 shows the overlapped beam patterns from the E-,D- and H-planes at 90 GHz. The beams match each other perfectly and are symmetric. This characteristic was observed for all the frequencies over the band, but only results for the 90 GHz are shown here to limit the size of this report.

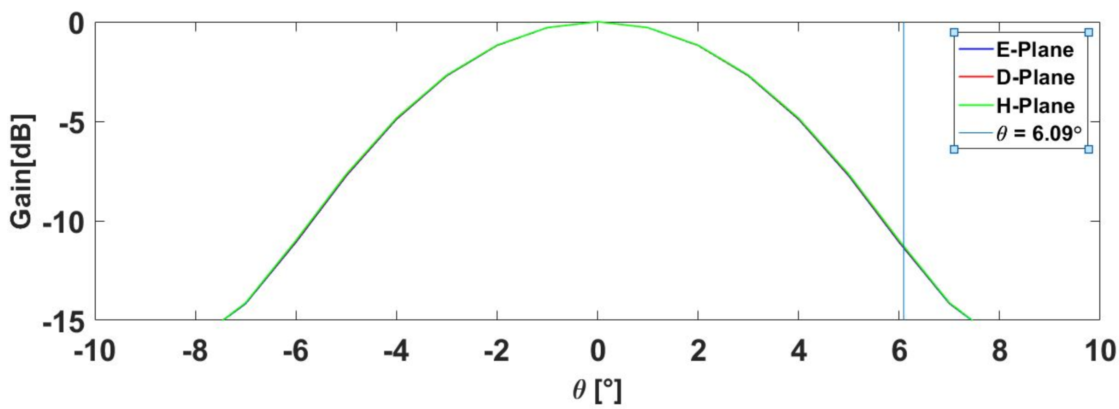

Figure 5.20: Beam patterns from the E-, D- and H-planes for the final corrugated horn design at 90 GHz have been overlapped to show beam symmetry which is a characteristic property for corrugated horns. The vertical line at θ= 6.09°shows the edge-taper specified for the thesis.

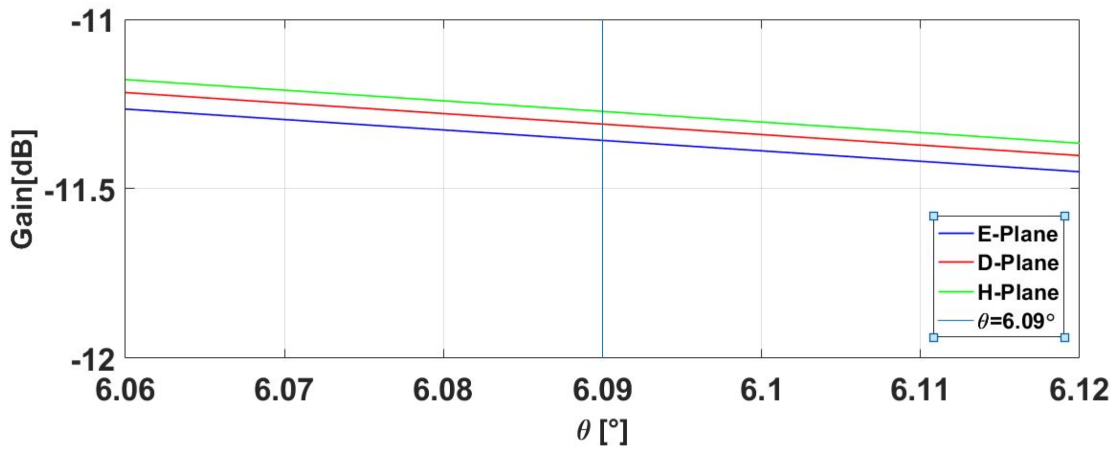

Figure 5.21: A magnified portion of Figure 5.20 around θ=6.09°, showing the beam pattern and taper in the E-,D- and H-Planes.

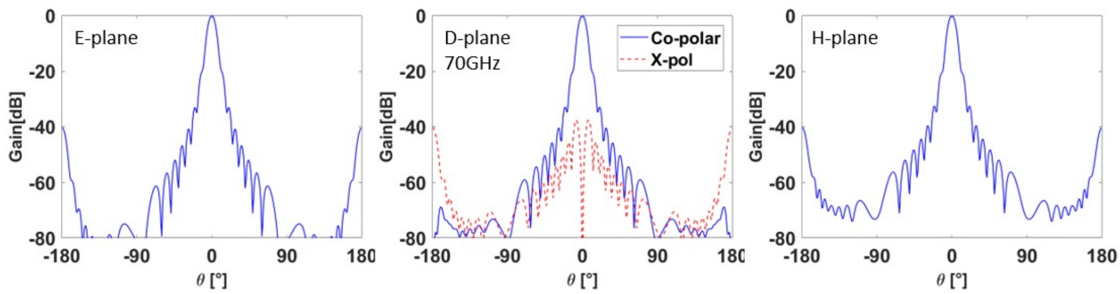

Figure 5.22: Simulated farfield beam patterns at 70 GHz in E-, D- and H-Plane for the final corrugated horn antenna.

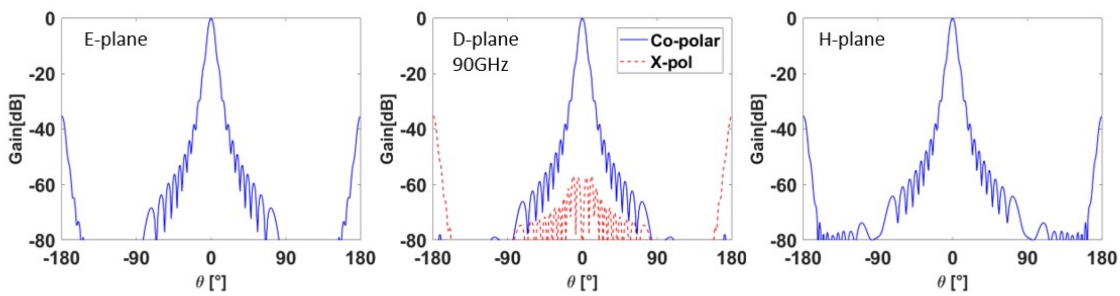

Figure 5.23: Simulated farfield beam patterns at 90 GHz for the final corrugated horn design.

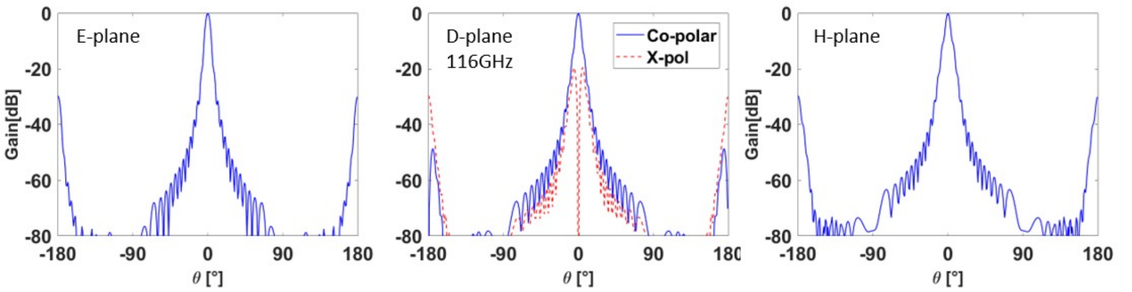

Figure 5.24: Simulated farfield beam patterns at 116 GHz in E-, D- and H-Plane for the final corrugated horn antenna.

5.4 Sensitivity and SEFD

Since there was a constraint of time on this project, a full sphere beam pattern integration of surrounding brightness temperatures could not be performed. However, the sensitivity of the single pixel feed can be approximated in an acceptable way. Section 2.4 presents how to calculate sensitivity in terms of system equivalent flux density. From equation 2.28,

$$T_{sys} = \eta_{rad} T_A + (1 - \eta_{rad}) T_P + T_{REC} \tag{5.1}$$

where,
T_A = antenna noise temperature
η_{rad} = antenna radiation efficiency
T_P = antenna physical temperature
T_{REC} = receiver noise temperature
From section 5.3.2, we know that η_{rad} is high, close to 100% and hence is assumed to be $\eta_{rad} \approx 1$. Therefore, (5.1) can be approximated as,

$$T_{sys} \approx T_A + T_{REC}. \tag{5.2}$$

For the 3mm/4mm application, the value of T_{REC} can be obtained from [39] which states that the average receiver noise temperature for the 4 mm band (E-band) is 40 K and for the 3mm band (W-band) is 55 K. We take an average value between these two and use this value as our T_{REC} which is 47.5 K. We now need to calculate T_A whose equation is given in Section 2.4. We assume that we only look at the zenith (θ=90°) to minimize the spill-over noise from the ground and focus on the atmospheric noise temperature, cosmic microwave background radiation $\sim$ 2.7 K is also ignored as it is small compared to atmospheric noise at these frequencies. We also assume that it is a 'perfect' day for observation in astronomical terms, i.e perfectly cloudless skies with cold weather which provides a more transparent atmosphere. We also assume that there is no spillover from the reflector to simplify our calculations. This assumption in reality is not true and generally, 10 K - 20 K noise comes from spillover. Then the antenna noise temperature, T_A can be approximated as the noise temperature coming from sky, T_{sky} and the atmospheric noise temperature, T_{atm}, $T_A \approx T_{sky} \approx T_{atm}$. From the Onsala handbook for the 20 m dish telescope [26], we obtain the Figure 5.25. From this figure we can obtain values for T_{atm} and calculate T_{sys} for our design. In practice, the system noise temperature depends on the design of the feed for both the antenna temperature, T_A and receiver noise temperature, T_{REC} and can never be ignored.

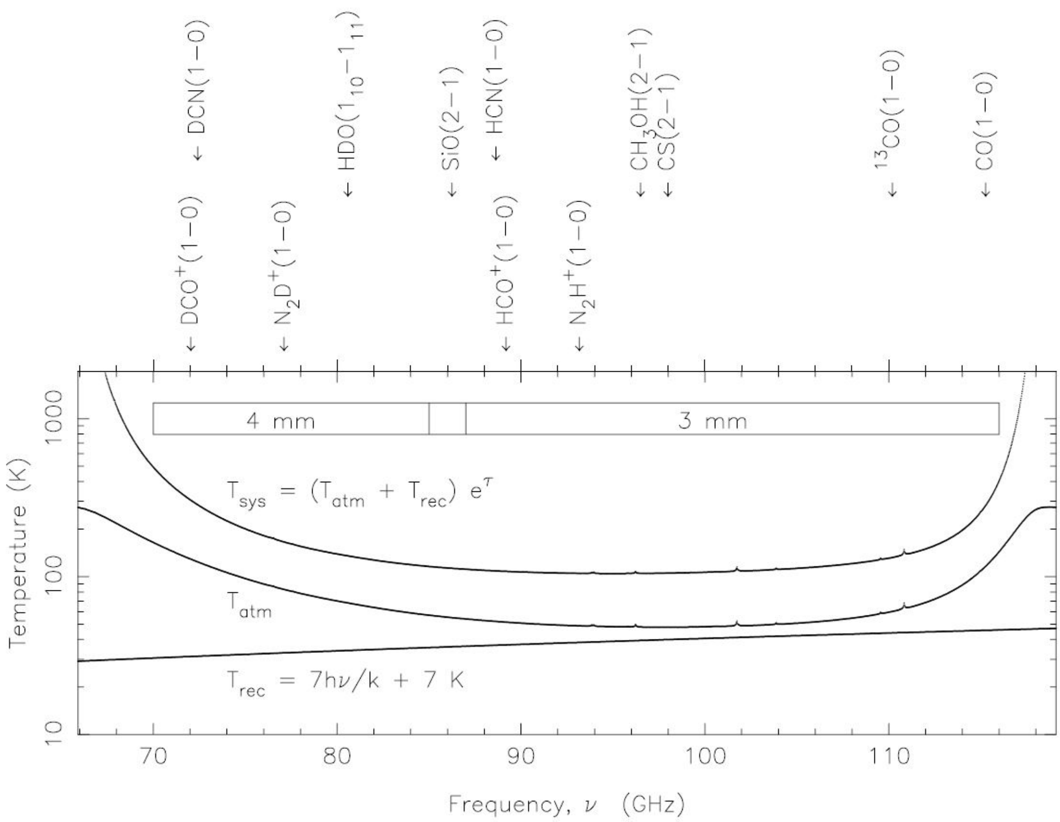

Figure 5.25: System noise temperature T_{sys}, receiver noise temperature T_{REC} and atmospheric noise temperature T_{atm} approximated for the Onsala 20 m radio telescope over the E-W Band (Source: Onsala Space Observatory [26]).

Effective aperture area, A_{eff} is nominally calculated as

$$A_{eff} = (\eta_{losses}) \times \eta_A \times A_{geom} \tag{5.3}$$

where, A_{geom} is the physical geometrical area of the dish and η_{losses} includes radiation and dish losses, but in this case we assume it as 1. For the purposes of this calculation we ignore the dish losses, to simplify (5.3) to (5.4). In reality, at such high frequencies, dish losses cannot simply be ignored as they are quite significant and affect performance.

$$A_{eff} = \eta_A \times A_{geom} \tag{5.4}$$

From here, SEFD for the dish can be calculated according to the equations given in section 2.4. Figure 5.26 gives us the approximated values of the sensitivity of the system, with and without the consideration of atmospheric opacity.

The parabolic shape of the graph illustrates well the difficulty of having good sensitivity for measurements at either end of the spectrum. The SEFD presented

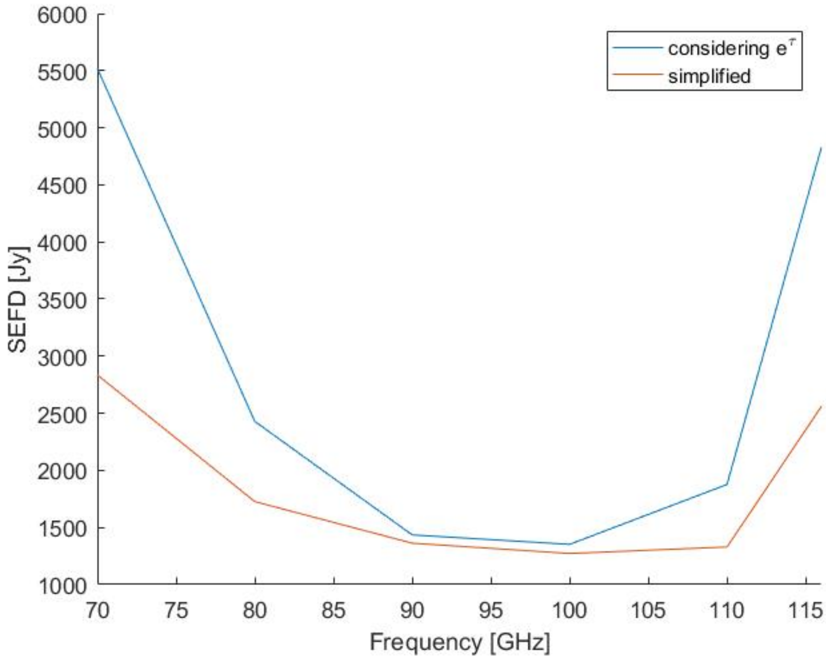

Figure 5.26: Approximated sensitivity values for the final corrugated horn design. The red curve shows the values when atmospheric opacity is not taken into consideration with the maximum sensitivity occurring at 1272.49 Jy at 100 GHz and the average sensitivity measuring 2100 Jy. The blue curve shows the sensitivity values when atmospheric effects are taken into account, which is a more realistic scenario, the maximum average sensitivity values at 3550 Jy.

is approximated with simplifications due to the system complexity and time constraints, and in these conditions, they meet our requirement specified for sensitivity (SEFD) in Section 3.7. If we use the T_{sys} values given in Figure 5.25 which takes into consideration the atmospheric opacity, e^{τ}, for our frequency band we see that the SEFD number for 70 GHz is approximately 5500 Jy and for 116 GHz it is 5200 Jy, whereas for 90 GHz it is $\approx$ 1600 Jy, shown in Figure 5.26. These values, specially for the extremes of our selected spectrum, are much higher than the ideal values we have calculated. In reality, the 20 m dish is covered with a radome which contributes to dielectric loss and scattering effect. The gravitational effect of the telescope tipping means that the shape of the parabolic reflector changes and pushes the sub-reflector with the structure. The anomalies cannot be compensated for perfectly. At such high frequencies, the dish surface also contributes significantly to losses. However, in this thesis we have assumed that the surface of the dish is near perfect which is not the case for the 20 m dish. However, since we do not have enough data for estimating these effects in our study, we accept the approximated values of sensitivity.

5.5 Existing Horn Designs for the E-W Band

There are several corrugated horn feeds that have been designed for the same frequency bands as used in this project. We discuss the results of one of these designs mentioned in the paper titled, "Design of a 67-116 GHz Corrugated Circular Horn for the ALMA Radio Telescope" by R.Nesti, G.Pelosi, S.Pilia and S.Selleri [40].
The paper documents an ultra-wideband circular corrugated horn feed designed for bands 2 and 3 of the ALMA radio telescope located in the Atacama desert in Chile. The bands cover frequencies from 67 GHz to 116 GHz with a chosen center frequency of 91.5 GHz and corresponding wavelength of 3.726 mm. The specifications of the design included an input reflection coefficient better than -30 dB, a cross polarization level lower than -30 dB over the whole band and an edge taper of -12 dB at 17 °at center frequency in the 45°plane.
The specifications were successfully met with a compact corrugated horn 52.08 mm in length and 17.98 mm wide aperture. It consists of a total of 46 corrugations, the transition region occurring in the first 32 corrugations. The attained reflection coefficient and cross polarization level are reported to be well below the -30 dB requirement, Figure 5.27 shows these results in dB as a function of frequency. Figure 5.28 show the radiation pattern of the ALMA horn at 91.5 GHz.

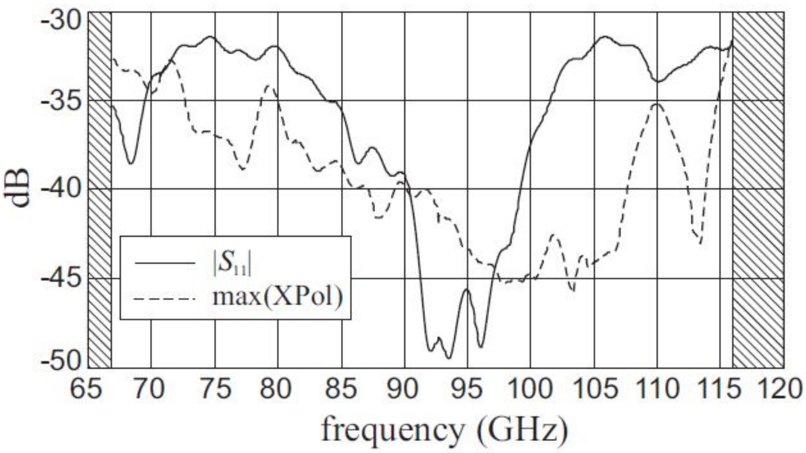

Figure 5.27: ALMA Horn input reflection coefficient,$|\ S_{11}\ |$ and maximum crosspolar level, max(XPol), in dB over the frequency band. Image Credit: [40]

The pattern is showed for the E-plane, H-plane as well as the 45°plane. We see good symmetry in the pattern in all the three planes which is a characteristic feature for the corrugated horn. The small inset image shows a magnification of the pattern around 17°. It is reported that the drop at 17°is 11.99 dB in the 45°plane which is very close to their requirement of 12 dB. The taper varies by ±0.2 dB in the E-plane and the H-plane. The phase centre variation over the band is shown in Figure 5.29. The variation is limited to around 4mm over the whole band.
If we do a comparative study of the design presented in the ALMA paper [40] and our final design, we will call it the Onsala design for the sake of comparison, has a higher input reflection coefficient in the lower half (between 70 and 90 GHz) of the band

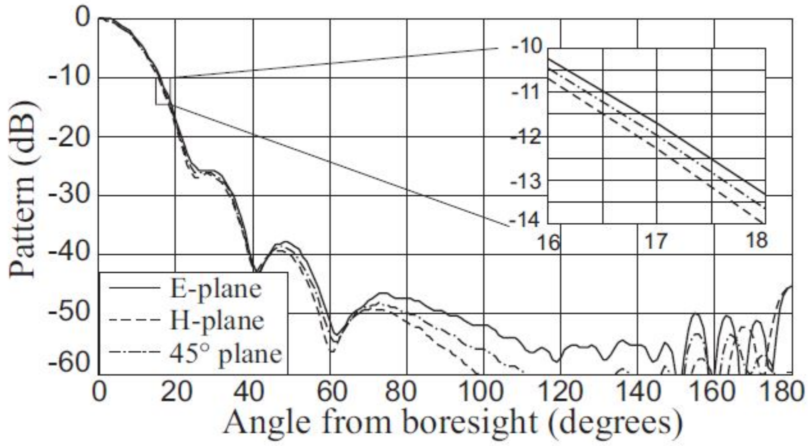

Figure 5.28: Gain pattern of the ALMA horn at 91.5 GHz in E-Plane, H-Plane and 45°plane. The inset image magnifies the graph around 17°to show the -12 dB taper in the 45°plane with an error of ±0.2 dB in the E-plane and H-plane. Image Credit: [40]

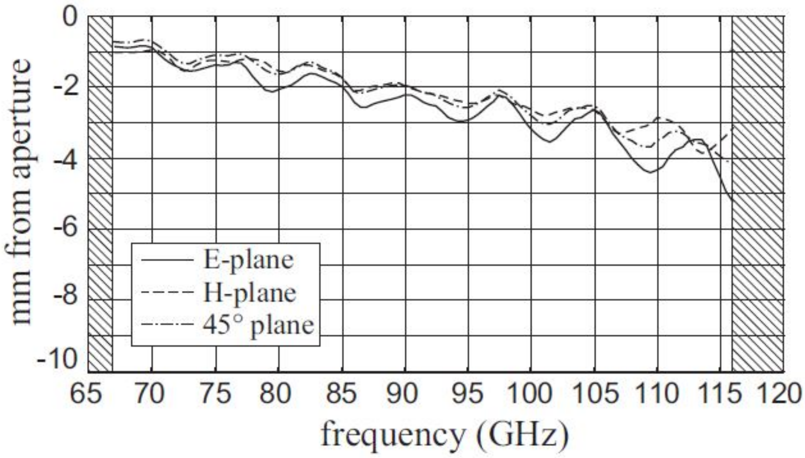

Figure 5.29: Phase center positioning of the ALMA horn on E-plane, H-plane and the 45°plane as a function of frequency. The values are presented in millimeters from the aperture with the negative values moving inwards the ALMA horn. Image Credit: [40]

and similar values for the upper half of the band (between 90 and 116 GHz). The Onsala design also does not meet the edge taper requirements completely whereas the ALMA design has the specified edge taper with a very small margin of error. So what is it that makes the Onsala design different and still acceptable? The Onsala feed has a more challenging to design half-subtended angle at 6.09°. This is difficult to achieve. However, the design procedure, simulations and results produced in this thesis show that, it is not impossible to design a corrugated horn feed with good performance to produce the narrow beam required for the 20 m dish.

6
Conclusions

We have documented and proposed a 1.66:1 wideband circular corrugated horn feed for the Onsala Space Observatory 20 m radio telescope. The feed is designed to be used in the 20 m Cassegrain type dish geometry. It covers frequencies between 70 - 116 GHz and achieves an average aperture efficiency of 65% over the whole band. The corrugated design presents an input reflection coefficient less than -15 dB over the entire band and is reasonably close at -11.356 dB to the required -12 dB edge taper at the small half-subtended angle of 6.09°at 90 GHz in the E-Plane. System equivalent flux density (SEFD) was evaluated in assumed ideal conditions as a measure of sensitivity of the corrugated feed system. When the atmospheric opacity is not taken into account, with the ideal maximum sensitivity value is 1272.49 Jy occuring at 100 GHz, while the average over the whole band is 2100 Jy. If the atmospheric opacity of the system is considered, which is the relatively more practical scenario, then the maximum average sensitivity is 3550 Jy, in both these scenarios, the set goals are achieved. The report also documents a smooth circular horn design which forms the basis of the corrugated horn design for this project.

The fundamental theory and equations used for the horn design were taken from the paper titled "Design of Corrugated Horns: A Primer" by Christophe Granet and Graeme L. James [29]. The design of the corrugations was carried out in MATLAB whereas the electromagnetic simulations of the smooth and corrugated horn were performed in CST Microwave Studio. The smooth horn design was important to analyze the performance of the horn and to optimize the various parameters necessary to achieve the specifications of our design. Corrugations were then introduced in suitable smooth horn designs and the results of the final selected designs for both the smooth horn and the corrugated horn were documented in this report.

The design approach as mentioned in [29] gives satisfactory results in terms of performance but results from the final corrugated horn design suggests that the mode converter located at the throat of the horn has some imperfections. The transition of modes from transverse mode to hybrid mode is not smooth and this causes the results between 70 GHz and 80 GHz to not follow the expected trend. Possibly, a different design approach needs to be considered to design the mode converter of the horn for improved performance.

The sensitivity results are also approximated and give the most ideal values that the designed final corrugated horn can achieve without atmospheric affects (which is not realistic). In reality, if we take into account various efficiencies and sub-efficiencies of the dish and the feed along with actual atmospheric conditions at the time of observation, the sensitivity will always be worse than the values presented in this thesis. A brief comparison was also done between the existing corrugated horn design for the ALMA telescope mentioned in [40] and our final corrugated horn design. It was concluded that, the corrugated horn designed for the ALMA telescope achieves slightly better overall performance and reasoned that the Onsala design has it's own extreme requirements due to which its performance is hindered.

The main challenge of the thesis was to create a corrugated horn for the extreme specification of achieving an edge-taper of -12 dB@6.09°at center frequency in the ϕ =0°plane. From all the results obtained, this thesis shows that the challenge was successfully met and the reported design can be further improved for better performance. Possible future improvements in the final design of the horn are suggested and development of the final corrugated horn design into a radio-camera feed is also documented.

7

Future Scope and Development

This project is part of a greater vision to develop a multi-pixel 'radio-camera' array for the Onsala 20 m radio telescope. Similar projects have been carried out for other telescopes around the world [41], [42]. A radio-camera fed reflector gives faster survey speeds with a wider field-of view. Some suggestions for further development of the array are given below,

- a study in the trade-off between field-of-view and sensitivity for the radio-camera is crucial to motivate whether an upgrade is reasonable. This would give answers to how much sensitivity is lost in favour of increasing the survey speed with a wider beam on the sky.
- a study in beam separation vs noise contribution would show how separated beams vs overlapping beams compare and how this would contribute to overlapping losses.
- effect of array configuration on beam shaping is also another important factor to consider.
- different antenna element instead of the corrugated horn could be used to create the array, e.g. bullet antenna - it can potentially reduce the cost of the whole array system.

The author also realizes that the horn design she has is good but can be greatly improved. Some suggestions are given below,

- An algorithmic optimization strategy could be used to further improve the performance of the design, maybe contribute towards better aperture efficiency. Since the corrugated horn consists of a large number of variable parameters, a broad optimization strategy such as those mentioned in [43] might be useful.
- The corrugations in the mode converter could be designed differently in order to shorted the length of the horn. The mode converter is a very important segment of the corrugated horn, as such it contributes to the total length of the design as well as its performance. Horizontal or axial corrugations as mentioned in [44] could have interesting effects on the length of the horn, return loss as well as the manufacturing process of the horn.
- Other profiling options could also be considered for better design. In this thesis, we only considered four profile options: exponential, hyperbolic, sinusoidal and xp profile. A lot of other profile options exist such as asymmetrical sine, tangential and linear. Gaussian profile has recently become more popular among horn designers due to it producing good symmetry in beam patterns [45]. Spline-defined profile has also come into limelight for its performance, however it takes a lot of computational power and efficient optimization algorithms [17].

Bibliography

[1] Nola Taylor Redd. *What is Astronomy? Definition and History.* URL: https://www.space.com/16014-astronomy.html.

[2] *The History of Astronomy.* URL: http://curious.astro.cornell.edu/people-and-astronomy/the-history-of-astronomy.

[3] *Astronomy in Everyday Life.* URL: https://www.iau.org/public/themes/astronomy_in_everyday_life/.

[4] *Nicholas Copernicus.* URL: https://starchild.gsfc.nasa.gov/docs/StarChild/whos_who_level2/copernicus.html.

[5] Tammy Plotner. *What is Galileo's Telescope?* URL: https://www.universetoday.com/15763/galileos-telescope/.

[6] *What are Radio Waves?* URL: https://www.nasa.gov/directorates/heo/scan/communications/outreach/funfacts/txt_radio_spectrum.html.

[7] *Karl Jansky.* URL: https://www.nrao.edu/whatisra/hist_jansky.shtml.

[8] Sancar J Fredsti. *A brief history of Radio Astronomy.* URL: http://www.astronomytoday.com/astronomy/radioastro2.html.

[9] *High Energy Astrophysics Picture of the Day.* URL: https://heasarc.gsfc.nasa.gov/docs/objects/heapow/archive/active_galaxies/cena_composite.html.

[10] *IAU List of important spectral lines.* URL: https://www.craf.eu/iau-list-of-important-spectral-lines/.

[11] *Onsala Space Observatory.* URL: http://www.chalmers.se/en/research%5C%5Cinfrastructure/oso/Pages/default.aspx.

[12] *Computer Simulation Technology.* URL: https://www.cst.com/products/cstmws.

[13] *MATLAB.* URL: https://se.mathworks.com/products/matlab.html.

[14] Per Simon Kildal. *Foundations of Antenna Engineering: A Unified Approach for Line-of-Sight and Multipath.* Kildal Antenn AB, 2015. ISBN: 9789163785146.

[15] Constantine A. Balanis. *Antenna Theory: Analysis and Design.* Wiley & Sons, Inc, 2016. ISBN: 9781118642061.

[16] Thomas A. Milligan. *Modern Antenna Design.* Wiley & Sons, Inc, 2005. ISBN: 9780471457763.

[17] Jonas Flygare. *A Wideband Quad-Ridge Flared Horn Feed Design for the Square Kilometre Array Band 1:Antenna Design, Simulation and Measurement.* 2018.

[18] A. D. Olver. *Corrugated Horns for Microwave Antennas.* Electromagnetic Waves. Institution of Engineering and Technology, 1984. URL: https://digital-library.theiet.org/content/books/ew/pbew018e.

[19] *The Radio Sky.* URL: https://public.nrao.edu/gallery321.

[20] *Radio Astronomy Lecture 1.* URL: https://web.njit.edu/~gary/728/Lecture1.html.

[21] *Radio Telescopes.* URL: http://abyss.uoregon.edu/~js/glossary/radio_telescope.html.

[22] *Radiometer Equation Applied to Telescopes.* URL: https://casper.ssl.berkeley.edu/astrobaki/index.php/Radiometer_Equation_Applied_to_Telescopes.

[23] R. Collin. "Aperture efficiency for paraboloidal reflectors". In: *IEEE Transactions on Antennas and Propagation* 32.9 (Sept. 1984), pp. 997–1000. ISSN: 0018-926X. DOI: 10.1109/TAP.1984.1143443.

[24] P.S. Kildal. "Factorization of the feed efficiency of paraboloids and Cassegrain antennas". In: *IEEE Transactions on Antennas and Propagation* 33.8 (Aug. 1985), pp. 903–908. ISSN: 0018-926X. DOI: 10.1109/TAP.1985.1143689.

[25] A.A Kishk A.D Olver P.J.B Clarricoats and L.Shafai. *Microwave Horns and Feeds.* The Istitution of Electrical Engineers, 1994. ISBN: 0852968094.

[26] A.O.H.Olofsson Lars E.B. Johansson and E. De Beck. *OSO 20 m Telescope Handbook.* 2016. URL: http://www.chalmers.se/en/researchinfrastructure/oso/radio-astronomy/20m/Documents/OSOman_31aug2016.pdf.

[27] James J. Condon and Scott M. Ransom. *Essential Radio Astronomy.* Princeton Series in Modern Observational Astronomy Ser. Princeton : Princeton University Press, 2016., 2016. ISBN: 9781400881161.

[28] *The Global 3mm VLBI Array.* URL: https://www.mpifr-bonn.mpg.de/1040999/Krichbaum-GMVA-export.pdf.

[29] C. Granet and G. L. James. "Design of corrugated horns: a primer". In: *IEEE Antennas and Propagation Magazine* 47.2 (Apr. 2005), pp. 76–84. ISSN: 1045-9243. DOI: 10.1109/MAP.2005.1487785.

[30] C. Granet. "Profile options for feed horn design". In: (2000), pp. 1448–1451. DOI: 10.1109/APMC.2000.926109.

[31] G. L. James and B. M. Thomas. "TE /sub 11/ to HE /sub11/ Cylindrical Waveguide Mode Converters Using Ring-Loaded Slots". In: *IEEE Transactions on Microwave Theory and Techniques* 30.3 (Mar. 1982), pp. 278–285. ISSN: 0018-9480. DOI: 10.1109/TMTT.1982.1131062.

[32] Graeme L. James. "Analysis and Design of TE11-to-HE11 Corrugated Cylindrical Waveguide Mode Converters". In: *Microwave Theory and Techniques, IEEE Transactions on* MTT-29 (Nov. 1981), pp. 1059–1066. DOI: 10.1109/TMTT.1981.1130499.

[33] *System Assembly and Modelling.* URL: http://cst2cm.acceptance.brimit.com/products/csts2/sam.

[34] *CST STUDIO SUITE 2012: System Assembly and Modeling.* URL: http://www.microwavejournal.com/articles/12117-cst-studio-suite-2012-system-assembly-and-modeling.

[35] *Asymptotic Solver.* URL: https://www.cst.com/products/cstmws/solvers/asymptoticsolver.

[36] *Circular Waveguides Sizes.* URL: https://www.cernex.com/PRODUCTS_NEW/Tech_info/Circular%20Waveguide%20Sizes.pdf.

[37] *Antenna Efficiency.* URL: http://www.antenna-theory.com/basics/efficiency.php.

[38] R. Maaskant et al. "Evaluation of the Radiation Efficiency and the Noise Temperature of Low-Loss Antennas". In: *IEEE Antennas and Wireless Propagation Letters* 8 (2009), pp. 1166–1170. ISSN: 1536-1225. DOI: 10.1109/LAWP.2009.2035148.

[39] Victor Belitsky et al. *A new 3 mm band receiver for the Onsala 20 m antenna.* Chalmers University of Technology, 2015. URL: http://proxy.lib.chalmers.se/login?url=http://search.ebscohost.com/login.aspx?direct=true&db=ir01368a&AN=cpl.220934&site=eds-live&scope=site.

[40] S. Pilia R. Nesti G. Pelosi and S. Selleri. "Design of a 67–116GHz corrugated circular horn for the ALMA radio telescope". In: *2017 IEEE International Symposium on Antennas and Propagation USNC/URSI National Radio Science Meeting.* July 2017, pp. 565–566. DOI: 10.1109/APUSNCURSINRSM.2017.8072325.

[41] Christopher Groppi et al. "SuperCam: a 64-pixel heterodyne imaging array for the 870-micron atmospheric window". In: *Society of Photo-Optical Instrumentation Engineers (SPIE) Conference Series.* Vol. 6275. Society of Photo-Optical Instrumentation Engineers (SPIE) Conference Series. June 2006, 62750O. DOI: 10.1117/12.671856. arXiv: astro-ph/0606061 [astro-ph].

[42] C. K. Walker. "SuperCam: A 64 pixel SIS receiver array for submillimeter-wave astronomy". In: *2015 IEEE MTT-S International Microwave Symposium.* May 2015, pp. 1–4. DOI: 10.1109/MWSYM.2015.7166873.

[43] Darragh McCarthy et al. "The optimisation, design and verification of feed horn structures for future Cosmic Microwave Background missions". In: *Infrared Physics & Technology* 76 (2016), pp. 32–37. ISSN: 1350-4495. DOI: https://doi.org/10.1016/j.infrared.2015.12.014. URL: http://www.sciencedirect.com/science/article/pii/S1350449515301808.

[44] J. Teniente et al. “Design Guidelines of Horn Antennas That Combine Horizontal and Vertical Corrugations for Satellite Communications”. In: *IEEE Transactions on Antennas and Propagation* 63.4 (Apr. 2015), pp. 1314–1323. ISSN: 0018-926X. DOI: `10.1109/TAP.2015.2390630`.

[45] Carlos Del Río et al. “Optimal horn antenna design to excite high-order Gaussian beam modes from TE0m smooth circular waveguide modes”. In: *Antennas and Propagation, IEEE Transactions on* 47 (Oct. 1999), pp. 1440–1448. DOI: `10.1109/8.793324`.